Test of models for electron transport in laser produced plasmas

D. G. Colombant*

Plasma Physics Division, Naval Research Laboratory, Washington, DC 20375

W. M. Manheimer

RSI Inc., Lanham, MD

M.Busquet

ARTEP Inc., Columbia, MD

Abstract

This paper examines five different models of electron thermal transport in laser produced spherical implosions. These are classical, classical with a flux limit f, delocalization, beam deposition model, and Fokker-Planck solutions. In small targets, the results are strongly dependent of f for flux limit models, with small f's generating very steep temperature gradients. Delocalization models are characterized by large preheat in the center of the target. The beam deposition model agrees reasonably well with the Fokker-Planck simulation results. For large, high gain fusion targets, the delocalization model shows the gain substantially reduced by the preheat. However flux limitation models show gain largely independent of f, with the beam deposition model also showing the same high gain.

PACS numbers: 52.57.Fg,52.65.Kj,52.25.Fi

*Electronic address: colombant@ppd.nrl.navy.mil

Report Documentation Page

Form Approved
OMB No. 0704-0188

1. REPORT DATE	2. REPORT TYPE	3. DATES COVERED
2005		**00-00-2005 to 00-00-2005**

4. TITLE AND SUBTITLE	5a. CONTRACT NUMBER
Test of models for electron transport in laser produced plasmas	5b. GRANT NUMBER
	5c. PROGRAM ELEMENT NUMBER
6. AUTHOR(S)	5d. PROJECT NUMBER
	5e. TASK NUMBER
	5f. WORK UNIT NUMBER
7. PERFORMING ORGANIZATION NAME(S) AND ADDRESS(ES) **Naval Research Laboratory,Plasma Physics Division,4555 Overlook Avenue SW,Washington,DC,20375**	8. PERFORMING ORGANIZATION REPORT NUMBER
9. SPONSORING/MONITORING AGENCY NAME(S) AND ADDRESS(ES)	10. SPONSOR/MONITOR'S ACRONYM(S)
	11. SPONSOR/MONITOR'S REPORT NUMBER(S)

12. DISTRIBUTION/AVAILABILITY STATEMENT
Approved for public release; distribution unlimited

13. SUPPLEMENTARY NOTES
This article appears in Physics of Plasmas and can be found at Phys. Plasmas 12, 072702 (2005)

14. ABSTRACT
This paper examines five different models of electron thermal transport in laser produced spherical implosions. These are classical, classical with a flux limit f, delocalization, beam deposition model, and Fokker-Planck solutions. In small targets, the results are strongly dependent of f for flux limit models, with small f's generating very steep temperature gradients. Delocalization models are characterized by large preheat in the center of the target. The beam deposition model agrees reasonably well with the Fokker-Planck simulation results. For large, high gain fusion targets, the delocalization model shows the gain substantially reduced by the preheat. However flux limitation models show gain largely independent of f, with the beam deposition model also showing the same high gain.

15. SUBJECT TERMS

16. SECURITY CLASSIFICATION OF:			17. LIMITATION OF ABSTRACT	18. NUMBER OF PAGES	19a. NAME OF RESPONSIBLE PERSON
a. REPORT **unclassified**	b. ABSTRACT **unclassified**	c. THIS PAGE **unclassified**	**Same as Report (SAR)**	**40**	

I. INTRODUCTION

In direct drive laser fusion, the laser irradiance is transformed mostly into electron thermal energy flux in the blow off plasma. This electron thermal energy flux is responsible for transporting the laser energy into the shell, ablating the outer part of the laser fusion pellet, and ultimately compressing and heating the inner part to generate a controlled fusion reaction. As such, electron thermal energy transport is extremely important in laser fusion. However often, heat conduction models used in fluid theory may not be valid because the mean free path of the conduction electrons is comparable to or longer than that temperature gradient scale length.

There have been a number of approaches to the theory in this case. Some of these are flux limiters [1] which phenomenologically reduce the heat flux to a fraction of its free-streaming value, delocalization models [2–8], the beam deposition model, which we have recently introduced [9], and Fokker-Planck modeling [7, 10–16]. Overwhelmingly, flux limiters have been used in most laser fusion simulations to address non-thermal electron transport. Its advantages have been its simplicity and its appealing intuitive nature. Although delocalization theories have been in the literature for nearly two decades, there seems to have been very little utilization of them in laser implosion simulations in the published literature. All the models described except for Fokker-Planck have been implemented in a fluid description which represents a huge saving in computational time. In this paper we test each of these theories by performing such fluid simulations of laser implosions. However, since we do not have access to a Fokker-Planck code, for these we rely on published calculations. We apply these theories to two different laser plasma configurations, a recent experiment on a laser implosion of a deuterium (DD) target [15], done at the University of Rochester with their frequency tripled OMEGA laser, and a high gain deuterium-tritium (DT) fusion target imploded with a MegaJoule Krypton Fluoride (KrF) laser [23].

Section II summarizes the different transport models. We note also that there are other models for transport inhibition. These are magnetic field generation perpendicular to the heat flow [17], and instability generated flux inhibition [18, 19]. We do not consider either of these two latter mechanisms here. Section III applies the different theories to the University of Rochester experiment. For the Fokker-Planck calculations, we rely on their published results which used a Fokker-Planck code coupled with their one dimensional (1D) fluid code

LILAC [20]. Our simulations are performed with the 1D version of the Naval Research Laboratory (NRL) code FAST [21]. This section contrasts the results for different transport models. Section IV summarizes the results for a high gain DT fusion target. Here, there are no Fokker-Planck simulations available for comparison. Section V draws conclusions. Since our beam deposition model has been modified since its original formulation [9], we have summarized additional work we have done on this model in the appendices. Appendix A summarizes recent improvements and changes to the model, and Appendix B describes some tests of the model to make sure it is internally consistent. One improvement we have yet to implement is the inclusion of the electric field. This will be presented in a future work.

II. MODELS FOR ELECTRON TRANSPORT IN LASER PRODUCED PLASMAS

In this section we review the different models used to describe electron transport in laser produced plasmas.

A. Classical transport

Classical transport has been summarized in Braginskii's book [24]. For an unmagnetized plasma, the thermal electron energy flux is given by

$$q = -\kappa \frac{\partial T_e}{\partial r} \tag{1}$$

where κ is the thermal conductivity and is given by

$$\kappa = 1.6 \times 10^{-12} \frac{n_e T_e \tau_e}{m} \gamma(Z) \tag{2}$$

where $\gamma(Z)$ varies from 3.2 for Z (charge state) = 1 to 12.5 for Z = ∞. Here n_e is the electron density in cm^{-3}, T_e is the electron temperature in eV and τ_e is the electron collision time in seconds. The numerical factor in front converts the temperature from eV to ergs. The electron collision time is given by

$$\tau_e = 3.5 \times 10^5 \frac{T_e^{3/2}}{n_e \lambda Z} \tag{3}$$

where λ is the Coulomb logarithm. Using the expression for the thermal flux given by Eqs.(1-3), one can numerically solve the fluid equations to calculate the laser implosion

characteristics. Since the thermal conduction is very high in a laser produced plasma, the electron temperature equation is almost always solved implicitly. This allows a numerically stable solution for the electron temperature equation, while taking time steps governed by the ion fluid velocity rather than the electron thermal velocity.

B. Flux inhibition

If we define the mean free path $\Lambda_e = v_e \tau_e$, where $2T_e = m_e v_e^2$, we can rewrite the thermal flux as

$$q = -\frac{\gamma(Z)}{2}\left(\frac{n_e m_e v_e^3}{2}\right)\frac{\Lambda_e}{L_T} \tag{4}$$

where L_T is the temperature gradient scale length. The idea behind the flux limit is that q cannot be larger than $n_e m_e v_e^{3/2}$, the so called free-streaming flux, so the flux is limited in some way if it were ever to get larger. In fact, one assumes that the flux is limited to some fraction of the free streaming flux denoted by f, that is $q < f n m_e v_e^3 \equiv q_{fs}$. Usually the best agreement with experimental results is obtained if f is taken to be rather small, typically between about 0.03 and about 0.1. The value 0.6 is considered to be the thermal value. All the calculations we performed for this work use a mean harmonic flux-limiter only (i.e. $q^{-1} = q_{class}^{-1} + q_{fs}^{-1}$). In the recent experiments performed at the University of Rochester, which we will examine here, their LILAC simulations concentrate on values of f between about 0.05 and 0.1 (they do not specify if they use a sharp cut-off or a mean harmonic flux-limiter although the difference is not very important[25]). While the flux limit has been used for about 30 years, and is straightforward to apply, to our knowledge there has never been a derivation of it in the reviewed scientific literature. To explain even different aspects of the same experiment or simulation, often different values of f are required [15]. In fact, to compare their results with Fokker-Planck simulations , the authors of Ref. 15 proposed a time dependent flux limit. To summarize, the flux limit has been in common usage for decades and has crept into accepted practice; most likely it has been grandfathered into the culture. Whatever other theories emerge, they will almost certainly be compared with flux limits of various values. It is reasonable to expect f to be less than unity, but to our knowledge there have been no first principles explanation of why a smaller value is reasonable. As we will see, the use of a small value gives fluid profiles which for the most part are reasonable, but do have significant unphysical features to them. In fact, earlier analytic, steady-state calculations [26] in a very different configuration show that the flux limit can produce unphysical results including even infinite slope and doubled-valued

temperatures. In our calculations, to be presented in the next section, we also see apparently unphysical results for a low flux limit value. However because of the fluid formulation of our calculations, it would not be possible to see double-valued fluid quantities. But when the analytic calculations show a double-valued temperature, it could be that the analogous fluid simulations would give results strongly dependent on the specific numerical algorithm [27].

C. Delocalization theories

In the 1980's a new class of theories emerged, the so called delocalization theories [2–8]. These theories all have the common feature of recognizing that since the mean free path can be long compared to a gradient scale length, the thermal energy flux is no longer determined locally but rather is determined in some way non locally. If the classical, Spitzer-Harm (SH) thermal energy flux given in Eq. (1) is redefined as q_{SH}, then all of the delocalization theories recalculate the nonlocal flux q as

$$q(x) = \int K(x, x') q_{SH}(x')\, dx' \tag{5}$$

where K is some kernel to be determined. The nature of these delocalization theories has been discussed more fully in Ref. 9. Reference 2 picks a physically reasonable kernel but without any real derivation. Reference 4 comes up with a kernel through an analytic solution of the Fokker-Planck equation in the region of the steep temperature gradient.

Ref.7 (and its extension to three dimensions, Ref.8) is what we focus mostly on and we shall refer to it as ES, the initials of its authors. Their logic and derivation is quite interesting, but the applicability of their model is possibly limited, as the authors themselves point out. What they do is take their Fokker-Planck code SPARK and perform a series of simulations. They set up a uniform plasma with temperature gradients, at various wave numbers but no pressure gradient, so fluid motion is minimized. They observe the time asymptotic decay of the temperature gradient. For small wave number they recover the classical result $\zeta_{SH}(k)$, a decay rate proportional to k^2. As the wave number k increases, they see that the damping rate ζ as a function of k has the form

$$\zeta(k) = \frac{\zeta_{SH}(k)}{1 + a|k|\Lambda_e} \tag{6}$$

where a is a number; they found that $a = 50$ fits the data best. This is roughly the ratio of the mean free path of heat carrying heat particles to that of thermal particles. As k

approaches infinity, the damping rate approaches a quantity proportional to k. Comparing their results with Refs. 2 and 4, they found that for these other theories, at large k, ζ approaches a constant, so that small wavelength fluctuations do not wash out, but all decay at the same rate. They argue that this is unphysical.

Once one has the heat conduction in the k domain, it is just a matter of Fourier transforming Eq. (6), to find q in the x domain. What they find is that the thermal flux has the form of Eq. (5), a simple convolution where they write out the kernel in their paper. It is in fact the convolution of the classical heat flux and the Fourier transform of the factor multiplying it in Eq. (6). This technique seems to have a great deal to recommend it, in that it directly comes from the Fokker-Planck equation, and ultimately arrives at a nonlocal expression for the heat flux.

However the authors themselves point out several difficulties with their approach. First of all, they want to use their expression for the heat flux in an implicit fluid calculation. For a high thermal conductivity, an implicit calculation involves inverting a tridiagonal matrix, since the second derivative, in matrix form is a tridiagonal. However a convolution of the form of Eq. (5) is a dense matrix, so one cannot do an implicit solution without inverting a dense matrix at every time step. Instead, what the authors of Ref. 7 do is to divide their heat flux, the Fourier transform of Eq. (6), by the classical heat flux, and then treat the quotient as a thermal conductivity in an implicit scheme. No other justification or discussion is given in Ref. 7. We note that an alternative is to simply use an explicit solution and pay the price in computing time if one can afford to do so. To our knowledge, this has not been attempted.

Another possible difficulty is that the heat flux can now be parallel to the temperature gradient instead of anti-parallel. For instance, if the classical heat flux is large and negative, the convolution may produce a heat flux, which is still negative, but in a region where classical theory would have it small and positive. Of course a heat flux parallel to the temperature gradient is a sure prescription for numerical instability when one uses a diffusion approximation, as the authors of Ref. 7 ultimately do. The authors believe that this will occur in regions with low density, where the heat flux is small compared to the maximum. They treat this by using classical heat flux wherever the heat flux is up the temperature gradient.

In addition, there are other potential difficulties not mentioned in Ref.7. Primarily, the

expression for heat flux is derived only for the case of linear perturbations in a homogeneous plasma. However, there are few cases in plasma science which are less linear, and less homogeneous, than the propagation of a thermal front in a laser fusion plasma. Reference 9 points out that different expressions for heat flux can be the same in the homogeneous, linear case, but may be very different in the more realistic case of nonlinear heat flux propagation in an inhomogeneous plasma.

In any case, the approach in Ref. 7 is well grounded in the Fokker-Planck equation, at least in certain limits. In these limits, it accounts for the large variation in particle velocity inherent in a kinetic description. Its standard formulation is planar, but despite that, it has been applied to spherical implosions, and we use that formulation here. We have applied this model to simulations of both the University of Rochester experiment, as well as to simulations of high gain laser fusion targets.

D. The beam deposition model

Another model which we have introduced [9] is the beam deposition (BD) model. As stated in Ref. 9, the goal is something more than a flux limit, but something less than a full Fokker-Planck simulation. The BD model is based on the fact that in the classical energy transport model, the velocity of the electrons which carry the flux is rather well defined. For an even simpler Krook collision model [9], the fractional thermal energy transport as a function of electron velocity is shown in Fig.1. A Fokker-Planck description gives about the same result. The negative energy flux at small velocity reflects the fact that there is a return current at low velocity which keeps the total current zero. However as Fig.1 shows, the flux is basically carried by particles between about 2.5 and 3 times $(2T_e/m_e)^{1/2}$.

For a fluid model to be valid, the mean free path of these energy carrying particles, Λ_e must be small compared to the temperature gradient scale length $L_T = T/[dT/dx]$. We denote the ratio Λ_e/L_T as α. Reference 9 shows that the validity of the fluid model for electron energy transport can be specified as $\alpha < 0.2$. The BD model is an attempt to describe the thermal conduction when this requirement for the fluid model is violated in certain, limited regions of the plasma. Each point where it is violated is taken as a source point for an electron beam. Thus the theory is formulated in terms of two radial parameters, r, and r_0, the position of the source point. We consider first a single source point, find the effect of modeling the transport as a beam source, and then get the total transport by summing over all source points.

The model approximates the thermal transport at a point r_0 with that of a beam of velocity v_b = 2.7 x $[2T_e/m_e]^{1/2}$ propagating down the temperature gradient. The beam's density, n_b is chosen so that the total energy flux is equal to the classical Spitzer-Harm thermal energy flux of the thermal plasma. Note that we model only the transport with the beam, not the thermal properties of the plasma. The beam propagates a momentum exchange mean free path down the temperature gradient. At this point, it is randomized in three dimensions. Instead of a beam, it becomes a hot electron plasma with density $n_h(r, r_0)$. To reiterate, r_0 is the source point, and $n_h(r, r_0)$ is the density of the hot plasma at position r and generated by the beam starting at r_0. This hot plasma diffuses into the main background plasma and heats it. It diffuses due to momentum exchange collisions with both ions and electrons, with collision frequency ν_p (in the theory, ν_p and many other parameters are functions of the two radial variables, r because the collision frequency depends on the local density and r_0 because it also depends on the velocity the electron had at its source point r_0. In terms of ν_p, the diffusion coefficient is given in Appendix A. For simplicity we will drop these dependences here). Also, as it diffuses, it also loses energy, but now only to the electrons. This collision frequency is ν_ϵ. After the velocity has decreased by a factor of 2.7 (i.e. a factor of e), it rejoins the main electron distribution and is lost from the hot plasma. The theory does not model the cooling in any other way except by having the hot electron ultimately rejoin the main plasma. That is, it models the cooling as a loss of beam particles.

Where this hot plasma exists, it heats the background plasma with heating rate ν_ϵ. Since this hot plasma has a source (the deposited beam), and a sink (the energy loss and background plasma heating), one can treat it as a steady state, as long as the electron time scale is very fast compared to the ion (i.e. fluid) time scale. Reference 9 very carefully checked this steady state approximation by comparing the relevant electron times with the fluid times. The former were always faster by several orders of magnitude. Hence in a fluid simulation, the beam deposition model can be regarded as a steady state process on the fluid time scale. It simply gives rise to additional heating and, as we will see, cooling of the electron fluid at various positions.

The BD model then solves the diffusion equation for $n_h(r, r_0)$ in spherical geometry analytically by making a WKB approximation. The hot electron density decays exponentially away from the point where it becomes the hot electron plasma. With the known hot electron density, one then calculates the heating rate. However the heating rate is balanced by the

cooling at the source of the beam. Clearly if a point in the plasma emits a beam, it must lose energy. For a single source point, the total heating rate $H^*(r, r_0)$ is given by

$$H^*(r, r_0) = \frac{1}{2}\nu_e(r, r_0)n(r, r_0)mv_b^2 - \frac{1}{2}n_b m v_b^3 \delta(r - r_0) \tag{7}$$

Here, n_b and v_b are both understood to be functions of only r_0. Since the beam from each source point moves forward a mean free path and deposits its energy, the source points are then a mean free path apart. The total heating is obtained by integrating Eq. (7) over all source points, assuming that these are a mean free path apart (i.e. the density of source points is Λ_e^{-1}). Reference 9 shows that the formulation is energy conserving. Hence for a single source point, the total heating rate given by the beam deposition model is shown in Fig.2 a). For the case of $\Lambda_e << L_T$, it is a simple matter to show that upon summing over source points separated by Λ_e, it reduces to the classical Spitzer-Harm value. That is a flux proportional to the temperature gradient at each point, moves a mean free path, and deposits its energy. Since every point is a source point, the heating rate of the plasma is proportional to the derivative of q.

The BD model, as we implement it does not attempt to totally reformulate the entire electron energy transport problem. To do so, one would have to solve in some way for the appropriate integral of H^* over the source points. Instead, it attempts to find a correction to classical thermal conductivity which accounts for the preheating due to the long mean free path. The assumption is that the heating and cooling which occurs within L_T of the source point is accounted for by classical theory. What classical theory does not account for is the heating, as specified by Eq. (7), but at a distance greater than L_T from the source point r_0. We include, then, only the heating predicted by Eq.(7) for $|r - r_0| > L_T$. However, since the theory is energy conserving, the heating far from the source point, must be balanced by a cooling near the source point. Thus instead of totally reformulating the theory of thermal energy transport, using Eq. (7), summed over source points, the BD theory uses Spitzer conductivity, but adds, for each source point a heating term, now denoted $H(r, r_0)$ and shown schematically in Fig.2 b). Notice that the preheat occurs both in front of and behind the source point. The cooling in the region of the source point is the way the BD model accounts for flux limitation. Indeed, as we will see, and have already seen, the BD model produces a heat front which lags behind that predicted by classical theory.

To complete the formulation, we sum the heating over all source points, so

$$H(r) = \int_0^\infty \frac{H(r, r_0)}{\Lambda_e(r_0)}\, dr_0 \tag{8}$$

The added heating is the way the BD model accounts for preheat; the added cooling is the way it accounts for flux limitation. As we will see, the additional heating is sufficiently small and well behaved that it can easily be included in an implicit solution of the electron temperature equation.

Let us now get a qualitative assessment of the importance of the new heating and cooling terms. First of all, the classical heating is given roughly by q/L_T within about L_T of the source point; we would like to compare the extra heating and cooling with this. The hot plasma density decreases exponentially away from its source with an e-folding rate given roughly by Λ_e^{-1} (a more accurate expression is given in Ref. 9 as well as in Appendix A here). From the point where the plasma begins to heat, the point marked with the star in Fig.2 b), the heating falls off in a distance Λ_e^{-1}. Hence an approximate value for the heating there is

$$H \sim \frac{q}{\Lambda_e}\left(exp - |\frac{L_T - \Lambda_e}{\Lambda_e}|\right) \tag{9}$$

The cooling, within the cooling region, is given roughly by $(\Lambda_e/L_T)H$. At what we consider to be the onset of the need for corrections to classical theory, $\alpha^{-1} = 5$, we see that the nonlocal heating from a single source is about 3% of the local classical heating. As we sum over regions of heating and cooling, the effect would most likely be further reduced. Hence, it appears that only for α's considerably larger than the onset value of 0.2 will there be a significant effect. As we will see, the α's can get considerably larger in a laser implosion, and there are indeed nonlocal effects.

While the BD model was mostly formulated in Ref. 9, in the intervening time we have made a number of improvements to the model since the initial formulation. These are described in Appendix A. Also we have made several checks of the model, and these are described in Appendix B.

To summarize, we feel that the beam deposition model is indeed more than a flux limit, but less than a Fokker-Planck solution. It can be incorporated simply in existing implicit calculations. It appears to capture the essential physics of both preheat and flux limitations. However it is based on a single velocity approximation to the thermal flux and in that sense neglects the complicated kinetic theory inherent in any complete description. Furthermore,

it separates out the thermal conduction from the density and pressure and treats it in a completely separate way. Nevertheless it does seem to capture much of the important physics, is simple to incorporate, and as we will see, it gives reasonable results.

E. Fokker-Planck Simulations.

One way of coming closer to the solution of the transport problem is to perform a numerical solution of the Fokker-Planck equation, solve for the electron velocity distribution, and thereby get all information including the transport. However solving the Fokker-Planck equation is an extremely time consuming process in the context of also solving for the laser implosion. For instance in Ref.15, the electron distribution is expanded out to include three terms in the Legendre polynomial expansion for the angular dependence of the electron distribution function. Each equation involves both x and v (the magnitude of the velocity), and each equation is constrained by a Courant condition involving a velocity several times the electron thermal velocity. Thus not only does the dimensionality of the equation increase, from (x, t) to (x, v, t) (with several equations added), but the time step is also reduced by two or more orders of magnitude. For this reason, Fokker-Planck simulations are extremely time consuming; for a laser implosion, they typically take days or weeks instead of the minutes or hours a more conventional fluid simulation takes. While several runs have been performed [7, 15, 16], it does not seem reasonable that one could ever do the number of separate simulations it would take to design a laser fusion target. In two or three dimensions, Fokker-Planck simulations would be even more prohibitive.

While Fokker-Planck simulations are indeed a much more accurate approach than any mentioned up to now, it is important to realize that there are limitations to their accuracy, even for the plasma portions of the target expansion where the Coulomb logarithm λ is larger than 1. First of all, they typically include only a small number angular eigenfunctions. Second, and more important, the collision integral only reduces to a Fokker-Planck equation for small angle collisions. This means λ must be large, in fact the Fokker-Planck formulation is only valid to order λ^{-1}. In a laser implosion, there are important regions of low temperature and high density, where λ is not large, there are many significant regions where it is less than 5, and even less than 3. Of course there are many additional important physical processes in parts of the target which the Fokker-Planck model does not treat at all. Several examples are radiation transport and Fermi degeneracy, all of which the fluid model treats with varying degrees of accuracy.

Thus while even a Fokker-Planck simulation has its own approximations, it is the best approach to the electron energy transport problem now available. At NRL we do not have access to a Fokker-Planck code. However we do compare our results to Fokker-Planck results by comparing to other published results. In Ref. 9 we compared our results with Ref .7. Here we compare our results principally to those published in Ref. 15.

III. RESULTS FOR THE UNIVERSITY OF ROCHESTER EXPERIMENT

Here we examine the effects of different transport models on the experiment described in Ref.15. The target is made of a 20 μm CH shell surrounding 15 atmospheres of D_2 gas. Its outer radius is 470 μm and it is irradiated by the OMEGA laser at a wavelength of 0.35 μm. The laser pulse rises to 25 TW in about 400 ps, stays at that level for another 500 ps and goes back to 0 at 1.3 ns. In Fig.3, we show, for the case of classical Spitzer thermal conductivity a) the electron temperatures at three different times, and b) the electron density at these times. These plots are, in most features, qualitatively similar for all other transport models. However there are significant differences in the details.

An important diagnostic, we find is the temperature profile at a particular time on one graph, and below it, the graph of α (that is Λ_e/L_T). In Fig.4 a) and b) we show this for the case of classical conductivity at a time of 1 ns. The figure shows only the part of the temperature profile which is inside the maximum temperature. There is a large blow off plasma, extending out well beyond a millimeter, which we do not show. The temperature decreases as a function of radius here, so the classical heat flux is outward (positive).

As is apparent from Fig.4, at 1 ns there are two temperature fronts propagating into the center, the ablation front, and a second front running out ahead of it. This second front is due to shock-front heating of the dense part of the target and propagating into a region of smaller density. It sits at the rear surface of the fuel and ultimately collapses into the center and contributes to the spark for burn calculations. As is apparent from .4 b), the α in the second front (which is the closest to the center) gets as large as 1, so a fluid description is certainly not valid there. However even in the main front, the α is as large as 0.5 over a significant region. Thus classical thermal conductivity produces a temperature profile for which the assumed fluid formulation is not valid.

Now let us see what a flux limit does. Shown in Fig.5 a) and b) are three displaced

graphs of the temperature and α as a function of r for flux limits of 0.05, 0.07 and 0.1. In our simulation, we use a harmonic expression for the flux limit as defined previously. Clearly, the use of a flux limit steepens the temperature profile in both fronts. The α in the main front can now become as large as 4, while the α in the second front increases above 1. In other words, use of a flux limit does not reduce the α, as one might hope or expect, but rather increases it! The need for a flux limit picks itself up by its own bootstraps. This steepening of the temperature front and the unphysical effects of a flux-limiter have already been observed in a different context [26].

Are these temperature profiles physical? Can a temperature front maintain itself if its thickness is only one fourth the mean free path of the of the heat carrying particles? It seems to us that the answer has to be no to both questions. Other more fundamental theories of flux limitation do give a physical explanation for how a temperature front can be maintained with a thickness less than the classical relevant mean free path. For instance some have speculated that the flux may be reduced because it propagates perpendicular to a self generated magnetic field [17]. Then the front must be thick compared to the Larmor radius, not the mean free path. Other theories had speculated on instability generated flux limitation [19]. Here the mean free path is anomalously reduced by the instability.

However the use of flux limitation [1], with no further theory or explanation gives no reason why the mean free path should be reduced, or why a temperature profile should be much steeper than the relevant mean free path. Therefore we conclude that the flux limit, whatever else it does correctly, does in fact generate temperature profiles which do not seem reasonable.

Now let us look at the delocalization model [7]. Figure 6 shows the analogous temperature and α plot at t=1ns. One thing apparent in Fig.6 is that the ES model predicts significantly more preheat in the core. Also, while it reduces the α in the leading temperature front (because it produces a uniform temperature there), it steepens the main front, increasing α to almost 2. However we do note that the ES model is not based on a fluid approximation, or on any expansion for small α. If the model is correct, these large α's may in fact be physical.

Figure 7 shows a different aspect of the model. It is a plot of the thermal flux as calculated by classical thermal conduction, and also as calculated by the convolution. Here the maximum radius is 1.5 mm. The Spitzer flux is very large around r=0.4 mm. The

flux calculated by the convolution in this region is much smaller (5 times smaller); however it is much larger than the Spitzer flux in other regions. The reason is that the maximum Spitzer flux contributes greatly to the convolution at other radii, while the small classical flux elsewhere reduces the large flux at r=0.4 mm . For smaller r, the flux is larger as well, especially at the foot of the large surge in qSH. It is this larger flux which is responsible for the large preheat in the center of the plasma.

What is just as interesting is the flux for larger r. For r greater than about 0.06 cm, the classical flux is small and positive, and clearly approaches zero at 1.5 mm. The convolution flux however remains significant (at about 25% of its maximum value) and negative all the way to 1.5 mm. Thus the convolution predicts a significant flux up the temperature gradient over a large region of the plasma. To maintain numerical stability, when actually integrating the temperature equation, the calculated flux must be replaced with the Spitzer flux over a very large region of the profile.

To summarize, the ES model steepens the temperature profile. Since the model is not based on a small α expansion, this is not necessarily unphysical. However the model gives a very large amount of preheat, and a very large region where the heat flux is up the temperature gradient. This region must be treated in a special way to maintain numerical stability.

The analogous plots for the BD model are shown in Fig.8 at t=1ns. The temperature profile lags behind the Spitzer profile, as we have discussed earlier. The α's are about the same as for classical transport. Thus unlike any other theory, the BD theory does not make this situation worse. Also, like the ES theory, the theory is not based on small α everywhere, but attempts to model the effect of larger α's in limited regions of the plasma. Thus the presence of larger α's in limited regions is not necessarily unphysical.

Regarding the Fokker-Planck theory, Ref.15 does not give temperature profiles, so we are unable to make any direct comparisons. However we can and will give summary data which includes the Fokker-Planck theory.

We now give some summary data for the different transport models. The University of Rochester has pointed out the importance of the time of peak DD neutron emission, or bang time [15]. In their calculations, they show that with their fluid simulations, they reproduce the bang time best with a flux limit of 0.07, a flux limit of 0.06 delays the bang time by about 200 ps. They use this to argue for a flux limit of 0.07. In Fig.9 we show bang time as a

function of flux limit. Also shown are the bang times for the ES, BD, FP and Spitzer-Harm (SH) calculations. As is apparent, there is a large variation of the bang time as a function of flux limit. The Spitzer case , ($f = \infty$), gives the minimum bang time. The beam deposition model gives a slightly larger time and all other transport models increase the bang time. The University of Rochester simulations find an even larger variation of bang time with f [15]. Thus if matching the bang time is the criterion for validity of a theory, it is almost certain that one could find an f to give a match. However in all likelihood, the value of f would be different from experiment to experiment. Rather than affirming the validity of a flux limit as a basic theoretical tool, this seems to us to cast doubt upon it. The experimental result agrees best with the FP and f=0.08 results in our case (f=0.07 for the Rochester simulations in ref.15).

Figure 10 gives the total DD neutron production as a function of flux limit and for the other theories. If the FP is regarded as the most accurate theory, then SH and BD give more, and ES gives more than half of what FP gives. However the experimental result shows neutron production nearly an order of magnitude less than what the FP calculation gives (from Ref.15, it is estimated at around 7.5×10^{10}). The authors of Ref.15 attribute this to the effects of asymmetry and a possible Rayleigh Taylor instability, which none of the theories model.

Finally, Fig.11 shows the laser light absorption fraction as a function of f as well as for the other theories. Again there is a very wide variation of absorption with f and no experimental value is given since none is shown in Ref.15. As f decreases, the electron temperature in the blow off plasma must increase in order that the absorbed laser flux is conducted to the core. This is also clear from Fig.5. However the higher the temperature of the blow off plasma, the less the absorption. That seems to be the explanation for the fall-off of absorption with decreasing flux limit.

As a conclusion to this section, only two quantities can be compared to their experimental values and those are the bang time and the total number of neutrons. The flux-limit, the delocalization model ES and the FP results all fall within the range of the bang time experimental result whereas the beam deposition and SH models fall somewhat outside of it. All models fail for the number of neutrons observed. Leaving the neutron measurement aside, it seems that the FP model with its more rigorous theoretical basis is a promising model, albeit an expensive one in terms of computing time, the ES model is adequate for

this type of comparison (we shall see that it does not do as well for high-gain targets) and the flux-limiter approach is not convincing because of its steep variation with f, the free parameter, right where the agreements occur. However, on this one example, the BD model seems to be too small a correction for the classical model.

IV. RESULTS FOR A HIGH-GAIN TARGET

In this section we briefly summarize another series of calculations, these for a MegaJoule, high gain laser fusion pellet. The laser wavelength is 0.25 μm. The target consists of a 5 μm plastic layer surrounding a 192 μm wetted foam ablator $[CH(DT)_{16}]$ and a 252 μm DT fuel core. The outer radius of the target is 1.794 mm and the total injected energy is 1.2 MJ; also a two-step zooming [23, 28] is used in order to increase the absorption efficiency. The implosion time for this target is around 17.5 ns and does not change very much with the transport model.

Shown in Fig.12 a) are the temperature profiles every 0.5 ns between 13 and 16 ns, and in Fig.12 b) the density profiles for the BD transport model. The total laser energy is 1.2 MJ, and the calculated gain is 120. Shown in Fig.13 are analogous plots for the delocalization (ES) model. There are several significant differences in temperature profiles. Principally the ES model gives much more preheat than the BD model. This reduces the gain from 120 to 2.2, a very significant drop for laser fusion. Also the temperature profiles for the ES model have steeper gradients in the main heat front, but also have a much larger region of no temperature gradient at the temperature maximum. This reflects the fact that since the ES model gets the transport from a convolution integral, there can be significant transport even in regions of no temperature gradient.

We have also tested the effect of the flux limit on the gain. Shown in Fig.14 is a plot of the gain as a function of flux limit, with the results for Spitzer, BD and ES also indicated. It is significant that all models except ES give about the same gain. A high gain fusion target is of course larger than the target used in the Rochester experiments. Thus we would expect gradients would be smaller and effects of anomalous transport reduced. In addition, we show in Fig.15 the maximum values of α for the main front and the second front as a function of the flux-limiter value. We see that in the main front the α's indeed remain small even for low values of f. However in the leading front, the maximum values of α

increase for decreasing values of the flux-limiter as before. The fact that the gain is nearly independent of the electron thermal conduction model (except for ES) as shown in Fig.14 seems to indicate that in spite of the changes to the temperature profiles brought out by the different models, spark formation is quite robust against those changes. This result in itself may be the most positive result of this work, namely that laser fusion does not depend on the details of electron thermal transport. However for laboratory experiments which do not reach the spark formation stages and which have been carried out for the past 30 years or so, it is an important component of modeling. In a most optimistic approach, it may be that electron conduction models needed to explain in a satisfactory way present and past experiments will not be needed for burn simulations. However, this is not guaranteed and only burn experiments will tell if the community has been right not to tackle with more determination this challenging problem. In the words of Ref. 26, 'flux-limiting does not provide an acceptable alternative to more detailed (kinetic) modeling for predictive plasma applications'.

V. CONCLUSIONS

We have tested a variety of transport models on both the Rochester experiment and also on a high gain fusion target. For the former comparison, the results depend rather sensitively on model, and basic parameters show a large variation with the applied flux limit. We have also compared the models to the two available experimental results - namely the bang time and the neutron production from DD reactions. The ES model showed a larger amount of preheat than did any of the other models, and had he worst agreement as regard the neutron output. On this one example, the BD model seems to be only a small correction to the classical SH model.

Regarding a high gain fusion target, all models except ES showed about the same gain. This latter model showed much lower gain, undoubtedly because of the large amount of preheat. The ES model gave an anomalously low neutron production, as well as an anomalously high preheat. However the BD, classical, and flux limit model (with a properly chosen f) agreed reasonably well with a Fokker-Planck calculation. This indicates to us that the ES model, at least as currently formulated, is the one to treat with most suspicion. If this model is in fact incorrect here, it may be that one could improve on it. For instance, if one

were able to do an explicit ES calculation, with the actual convolution integral, rather than a diffusion approximation to it, it may be that it would give better results. If so, this would be good news for laser fusion, because it would bring it into agreement with all other models which give higher gain.

The insensitivity of gain with transport model (except for the ES model) means that for a high gain target, spark formation does not depend on the details of electron transport modeling. This optimistic view need however to be confirmed.

Acknowledgments

This work was supported by DOE. We would like to thank Dr. Jacques Delettrez for providing us with additional information on the Rochester experiment and simulation.

Appendix A. Improvements in the BD model

As we have mentioned, this work involves not only a comparison of different transport models, but also the further development of our own BD model. In this appendix we enumerate the improvements made to the model and theory.

1. The diffusion coefficient

In Ref. 9, the diffusion coefficient was written in Eq. (7) as

$$D(r, r_0) = \frac{v_b^2}{\nu_p(r, r_0)} \tag{10}$$

where v_b is understood to be a function of r_0. ν_p is a function of both r and r_0 because, as the theory is formulated, the velocity of the particle is understood to be defined as that at its source position, while the density defining the collision frequency is defined at r, wherever the particle is. Equation (10) is valid for a one dimensional plasma. For a three dimensional plasma, which the beam becomes once it is randomized in angle,

$$D(r, r_0) = \frac{v_b^2}{3\nu_p(r, r_0)} \tag{11}$$

which we now use.

2. Treatment of the center

The diffusion equation in spherical coordinates, as written out in Eq. (8) of Ref. 9 is

$$\frac{1}{r^2}\frac{\partial}{\partial r} r^2 D(r, r_0)\frac{\partial n_h(r, r_0)}{\partial r} - \nu_\epsilon(r, r_0) n_h(r, r_0) + n_b \frac{r_0^2}{r^2} v_b \delta[r - r_0 - s\lambda_p] = 0 \tag{12}$$

where s is plus or minus one, it takes on the opposite sign of the temperature gradient. In Ref. 9, we used as the WKB solution for Eq. (13)

$$n_h(r,r_0) = \frac{a(r_0)}{r[\nu_\epsilon(r,r_0)D(r,r_0)]^{\frac{1}{4}}} exp - \left| \int_{r_0+s\lambda_p}^{r} \left(\frac{\nu_e(r',r_0)}{D(r',r_0)} \right) dr' \right|^{\frac{1}{2}} \tag{13}$$

Here, A is a normalization chosen to conserve energy. Equation (13) has a divergence at the center (r=0). The total number of particles is finite, because it is an integrable singularity. However since the particle flux is proportional to the gradient of the density, there is a particle source, and therefore an energy source at the center. Because of this, our treatment in Ref. 9 usually had trouble as the heat front approached the center. However the proper boundary condition at the center is not to use an exponential which decays away from the source, but rather a hyperbolic sine for the inner solution. If the source point $r_0 + s\lambda_p$ is far from the center, there is no difference between the results. However as the source point approaches the center, the use of the sinh properly removes the singularity in n_h, i.e. the artificial energy source there.

3.Reflection about the center

Reference 9 did not consider what happens if after moving a distance λ_p, the radius became negative (those source points were eliminated). A simple physical argument shows that if a point moves to negative r one should simply use that value but with positive r. In other words, we reflect the negative r position about the center. This is implemented in the current formulation.

4. The integrated mean free path

In the BD model, before the beam is randomized in angle, it moves a distance λ_p down the temperature gradient. However often, the beam moves into a very inhomogeneous plasma, and the mean free path at its origin may be rather different from the mean free path a short distance away. Any of the density and temperature profiles shown in Sections III and IV show that this could well be true. Accordingly we redefine the mean free path to take into account the variation of plasma parameters along the path. That is, λ_p is now defined as

$$\int_{r_0}^{r_0+\lambda_p} \frac{\nu_p(r',r_0)}{v_b}\, dr' = 1 \tag{14}$$

5. The beam velocity

Reference 9 estimated the beam velocity by eyeballing Fig.1 and came up with the result $2.6[2T_e/m_e]^{\frac{1}{2}}$. Now we have regarded the velocity derivative of Fig.1 as the beam distribution

function. To define a single number characterizing the beam, we calculated the average mean free path of the distribution function, proportional to the fourth velocity moment and have used this. This changes the 2.6 factor to 2.7.

6. The cooling profile

Figure 2 shows that a part of the BD theory is a cooling of the plasma near the source point. Whenever one cools the fluid in a numerical simulation, there is always the danger that one may find an unphysical result of a negative temperature. Whenever the temperature becomes negative at any point in the simulation, the negative value is replaced with a small floor temperature (generally 0.1 eV). If this is implemented, clearly the energy conserving nature of the formulation is lost, and the plasma gains energy. In Ref. 9, we kept track of the number of times we implemented this floor temperature to replace a negative temperature. It hardly ever happened. However we have made one change to further reduce this possibility. As formulated in Ref. 9, the cooling was uniform throughout the cooling region. If within this cooling region, one portion of it has much smaller energy density than another, this former region is much more likely to have a negative temperature after the cooling algorithm is applied. To reduce the possibility of this, we have replaced the uniform cooling model with a model where the cooling is proportional to energy density instead of uniform. Implementing this new model, we have never yet run into a negative temperature at any point in the fluid simulation.

7. The definition of L_T

In any theory, L_T is most naturally defined as $L_T = T/T'$. As formulated in Ref. 9 an additional condition was used, $L_T = Min[T/T', L_2]$ where L_2 is the distance to the nearest point up or down the gradient where the temperature changes by a factor of 2. This gave the possibility of different definitions of L_T, depending on whether one goes up or down the gradient. Our experience has that the original, and simplest definition, $L_T = T/T'$ works best. This is what is now used.

Appendix B. Checks on the BD model

We have made a number of checks on the internal and the external consistency of the BD model. We have used the Rochester target for these tests. Since in most respects, parameters for the BD model are similar to the SH model, we have used as a check the DD

neutron production, the diagnostic showing the greatest difference. These results appear in Fig.16. Recall that the BD model predicts about 50% more neutrons than the classical model.

We have first checked on the DD neutrons as a function of beam velocity (Fig.16 a)). As the beam velocity decreases, the mean free path decreases as v_b^4. Thus at lower velocity, less and less of the exponential tail of the hot electron distribution extends beyond L_T from the source point. Hence we should approach the classical value as v_b decreases. We have found that as v_b decreases, we recover the classical result at $v_b = 2.5v_e$. As v_b increases, neutron production increases. It levels off at about $v_b = 2.7v_e$ and is reasonably constant, but with some fluctuations, up to $v_b = 3v_e$. Hence the results, for thermal plasmas, are not very sensitive to what one takes as the beam velocity, although $v_b = 2.7v_e$ is the proper choice as noted in the previous appendix.

The next check we have made is the neutron production dependence on the extent of the cooling region. Recall that in the model, so far we have not evaluated the integral of the actual heating over source points. Instead we used the heating beyond L_T for each source point and balanced it with cooling near the source point. As one uses values larger than L_T, ultimately one should recover the classical result. In fact we see that we recover the classical result for $2L_T$. However when we reduce the cooling region further, the neutron production begins to drop again, ultimately approaching the classical result for $0.5L_T$. This may be due to the fact that for a reduced cooling region, the corrections in the temperature near the source point are larger in amplitude and shorter in spatial extent. Since the next step in the temperature calculation is a diffusion step, these corrections are more easily erased than in the previous case. And the solution will relax to the classical one faster. In any case, L_T is certainly the choice indicated by theory.

Finally, we made a check when we varied the criterion for the existence of source points, that is we varied α. In Fig.16 c) we vary α between 0.01 and 1, a change of two orders of magnitude (the default value is 0.2). The main feature of that curve is that the neutron production does not change drastically with this parameter. In the limit of fewer source points ($\alpha = 1$), we recover the classical result as expected. In the opposite case ($\alpha = 0.01$), there are many source points, very often adjacent, and it may be that the cancellations between overlapping neighboring heating and cooling regions give rise to a short wavelength noise which is strongly damped out by the next diffusion step as alluded to above, hence

the recovery of the classical result.

To summarize, where the BD model should approach the classical value it does so smoothly. For some of the tests, it does so in the opposing limit as well. This could be because in these limits, the theory sets up short wavelength fluctuations which are quickly smoothed by the subsequent diffusion. However for each of these cases, theory does indicate particular values, $v_b = 2.7v_e, L_T = 1$ and $\alpha = 0.2$. It is also notable that DD neutron production does not change very much as these parameters vary. Hence the BD theory is unlike a flux limit. None of the theory's parameters can be varied to match experimental data.

---

[1] R.C. Malone, R.L. McCrory and R.L. Morse, Phys. Rev. Lett. 34, 721 (1975)

[2] J.F. Luciani, P. Mora and J. Virmont, Phys. Rev. Lett. 51, 1664 (1983)

[3] J.R. Albritton, Phys. Rev. Lett. 50, 2078 (1983)

[4] J.R. Albritton, E.A. Williams, I.B. Bernstein and K.P. Swartz, Phys. Rev. Lett. 57, 1887, (1986)

[5] P.A. Holstein and A. Decoster, J.Appl. Phys., 62, 3592(1987)

[6] P.A. Holstein, J. Delettrez, S. Skupsky and J.P. Matte, J.Appl. Phys. 60, 2296 (1986)

[7] E. M. Epperlein and R.W. Short, Phys. Fluids B 3, 3092 (1991)

[8] G.P. Schurtz, P.D. Nicolai and M. Busquet, Phys. Plasmas 7, 4238 (2000)

[9] W. Manheimer and D. Colombant, Phys. Plasmas, 11, 260 (2004)

[10] A.R. Bell, R.G. Evans and D.J. Nicholas, Phys. Rev. Lett. 46, 243 (1981)

[11] J.P. Matte and J. Virmont, Phys. Rev. Lett. 49, 1936 (1982)

[12] J.P. Matte, T.W. Johnston, J.A. Delettrez and R.L. McCrory, Phys. Rev. Lett. 53, 1461 (1984)

[13] E.M. Epperlein, G.J. Rickard and A.R. Bell, Phys. Rev. Lett. 61, 2453 (1988)

[14] F. Vidal, J.P. Matte, M. Casanova and O. Larroche, Phys. Plasmas 2, 1412 (1995)

[15] A. Sunahara, J.A. Delettrez, C. Stoeckl *et al*, Phys. Rev. Lett. 91, 095003 (2003)

[16] A.Nishiguchi, K.Mima, H.Azechi *et al*, Phys. Fluids B 4, 417 (1992)

[17] J.A. Stamper, Phys. Fluids 19, 758 (1976)

[18] W.M. Manheimer, Phys. Fluids 20, 265 (1977)

[19] W.M. Manheimer, D.G. Colombant and B.H. Ripin, Phys. Rev. Lett. 38, 1135 (1977)

[20] M.C.Richardson *et al*,in *Laser Interaction and Related Plasma Phenomena*, edited by H.Hora and G.H.Miley (Plenum Publishing, New York, 1986), Vol.7, p.421

[21] J.H. Gardner, A.J. Schmitt, J.P. Dahlburg *et al*, Phys. Plasmas 5, 1935 (1998)

[22] L. Spitzer, Jr. and R. Harm, Phys. Rev. 89, 977 (1953)

[23] S.E. Bodner, D.G. Colombant, A.J. Schmitt and M. Klapisch, Phys. Plasmas 7, 2298 (2000)

[24] S.I. Braginskii, Transport Processes in a Plasma (Consultants Bureau, New York, 1965)

[25] V. Goncharov (private communication)

[26] M. Day, B. Merriman, F. Najmabadi and R.W. Conn, Contrib. Plasma Phys. 36, 419 (1996)

[27] W.M. Manheimer, M.Lampe, R.W. Clark *et al*, Phys. Fluids 19, 1788 (1976)

[28] R.H. Lehmberg and J. Goldhar, Fusion Technol. 11, 532 (1987)

Figure captions

Fig.1 Fractional heat flux vs. electron velocity in the Krook model.

Fig.2 A Heating term in the beam deposition model for a source point r_0 deposited a mean free path λ away. B Heating and cooling terms for the same source point. Note that the cooling term is not spatially uniform but is proportional on the internal energy density of the plasma.

Fig.3 Typical temperature and density profiles at various times for a Spitzer conductivity for the Rochester experiment.

Fig.4 Temperature and α profiles at t=1ns for Spitzer heat conductivity.

Fig.5 Same temperature and α profiles for various values of a flux-limiter model of heat conduction at t=1ns. Note that the temperature profile steepens up and alpha increases for lower values of the flux limiter parameter.

Fig.6 Same temperature and α profiles for the delocalization model of Epperlein-Short (ref.7). Note the preheating of the center and the flattening of the temperature profile near its maximum.

Fig.7 Heat flux for Spitzer heat conduction and delocalization models. Note that in the case of the delocalization model, the maximum of the heat flux is reduced but also the heat flux extends beyond its classical range and never changes sign in the blow-off plasma.

Fig.8 Temperature and α profiles for the beam deposition model at t=1ns. This result is closest to Spitzer heat condcution model although it is lagging behind Spitzer model in time.

Fig.9 Bang time for the University of Rochester experiment as a function of flux limiter value. Also indicated are the results for the other models and the experimental value. Note the extreme variation of results given by the flux-limiter model.

Fig.10 DD neutron production as a function of the flux limiter parameter for the University of Rochester experiment. Results for the other models are shown as well as the experimental result.

Fig.11 Laser absorption fraction for the Universuty of Rochester experiment as a function of the flux-limiter value and for the other models. Again, the largest variation occurs for the flux-limiter model.

Fig.12 Temperature and electron density profiles at various times before the implosion for the beam deposition model. The gain is 120 for this case.

Fig.13 Same graphic for the delocalization model (Epperlein-Short). The gain is very low (G=2.2) because of the preheat in the core of the target.

Fig.14 Gain vs. flux-limiter values for the high-gain pellet. Note the small sensitivity of the results on the value of f.

Fig.15 Maximum values of the parameter α in high-gain targets for various values of the flux-limiter. Again, these values increase for both shock fronts for smaller values of f.

Fig.16 Sensitivity of physical parameters in the beam deposition model on the total number of DD neutrons in the University of Rochester experiment.

Fig.1

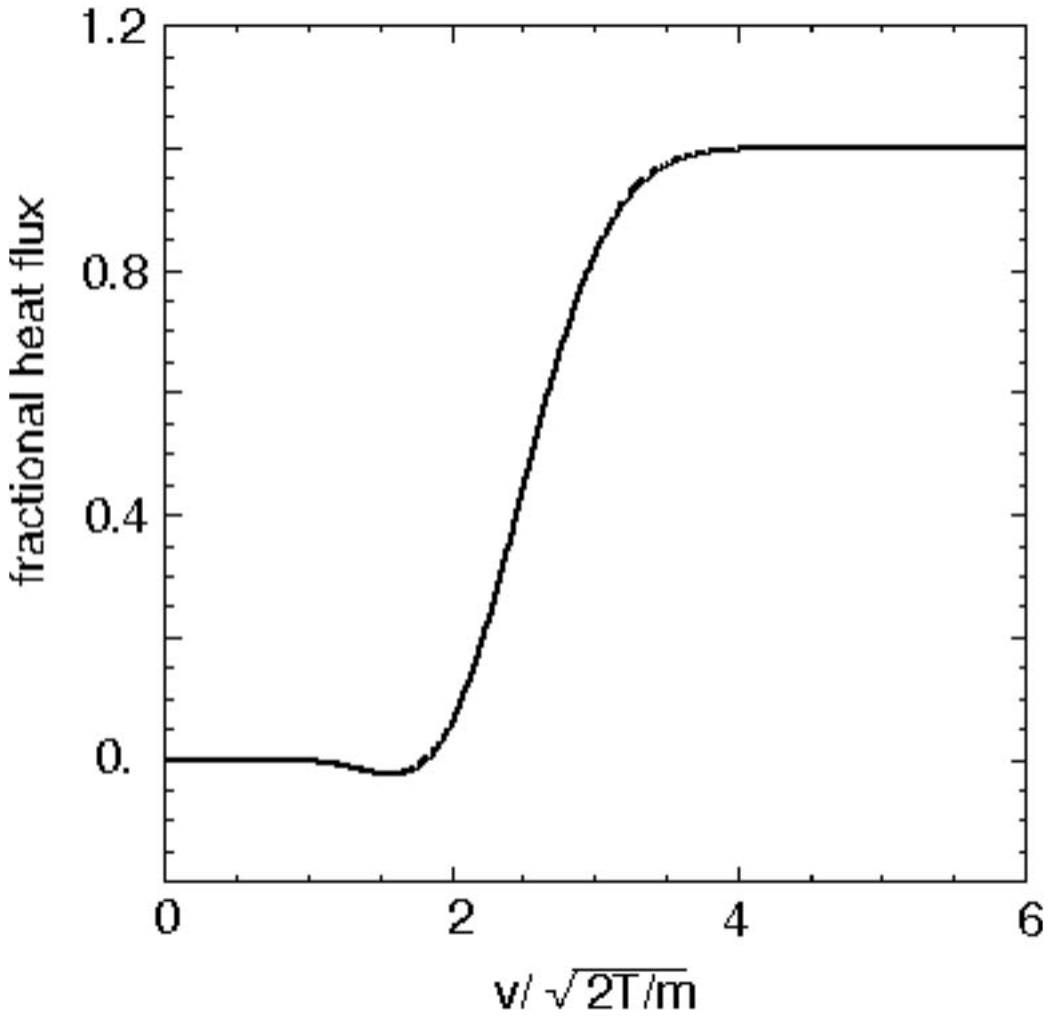

Fig.2

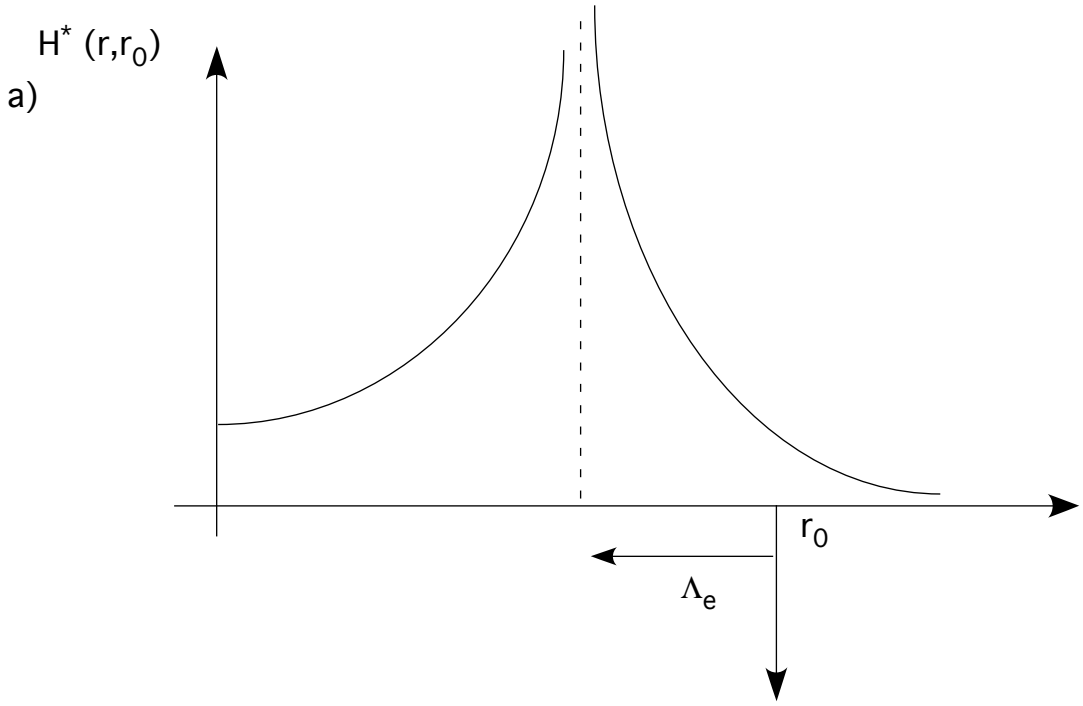

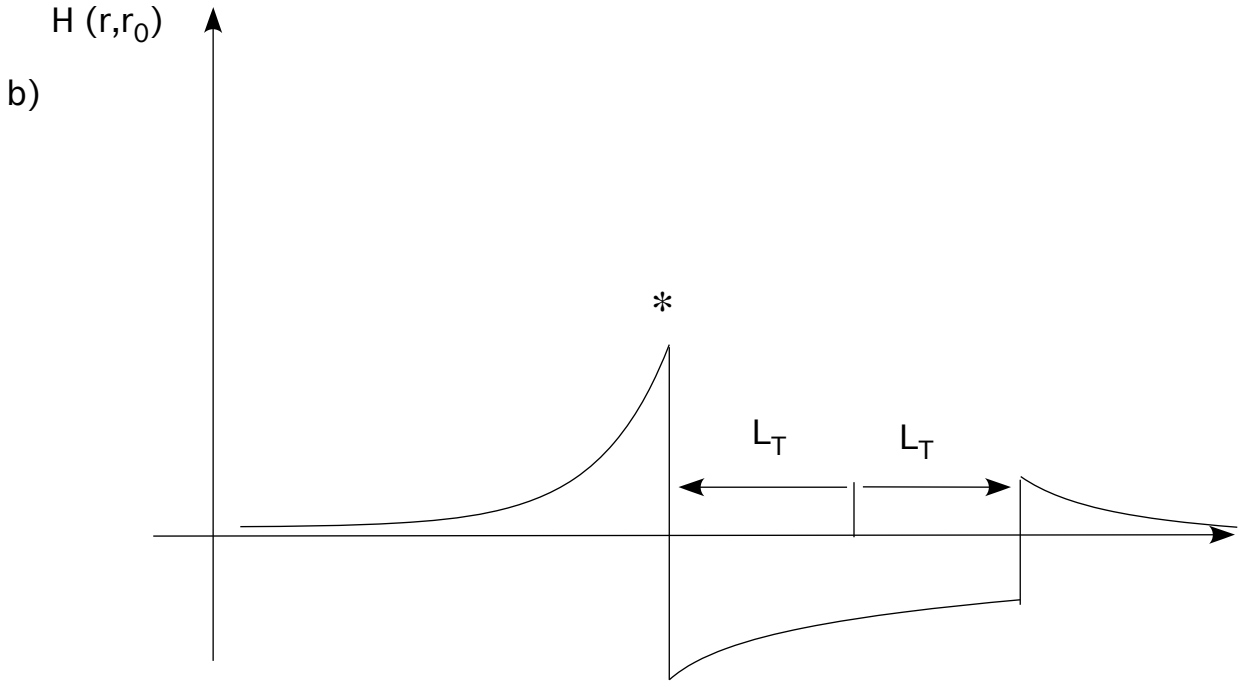

Fig.3

T vs. r at different times

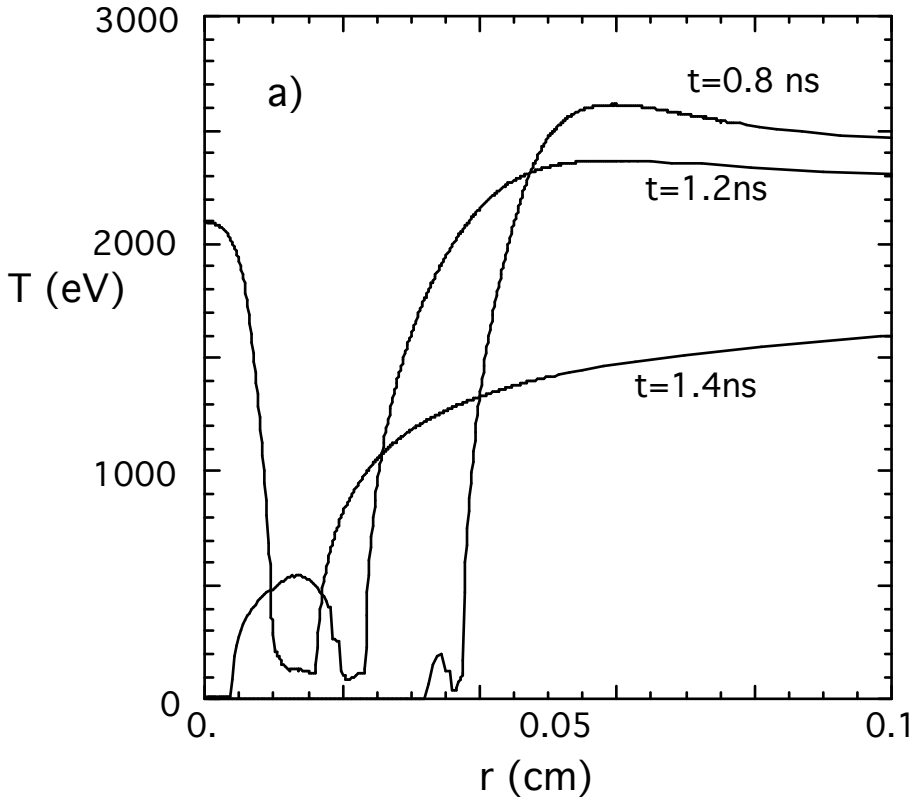

ρ vs. r at different times

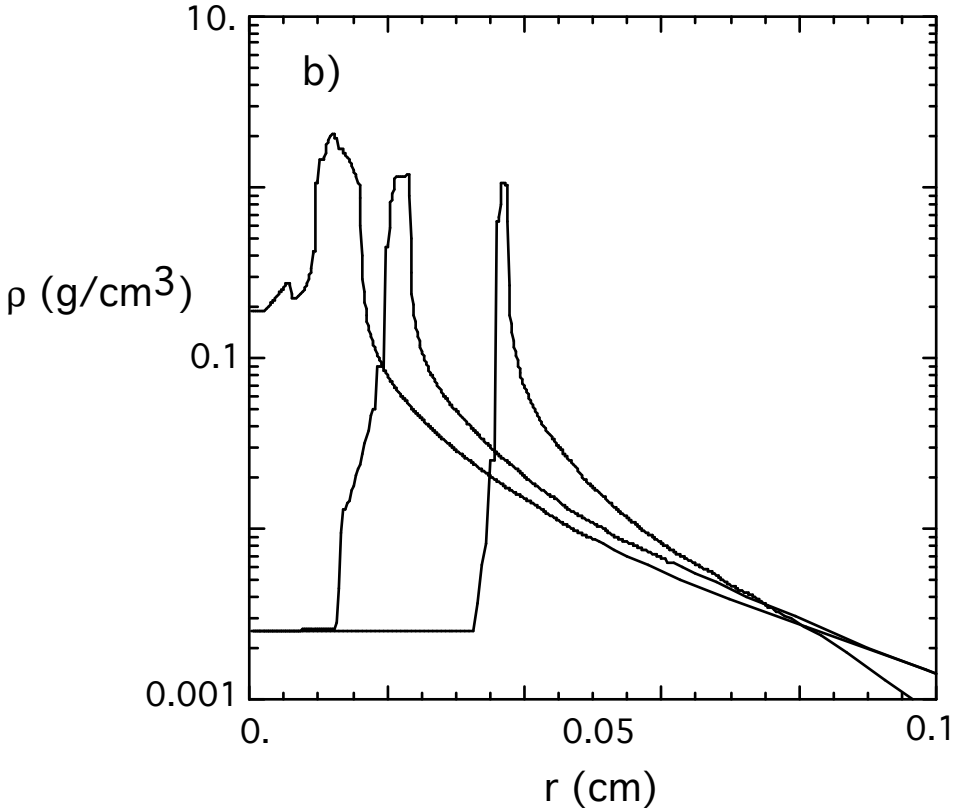

Fig.4

Spitzer at t= 1ns

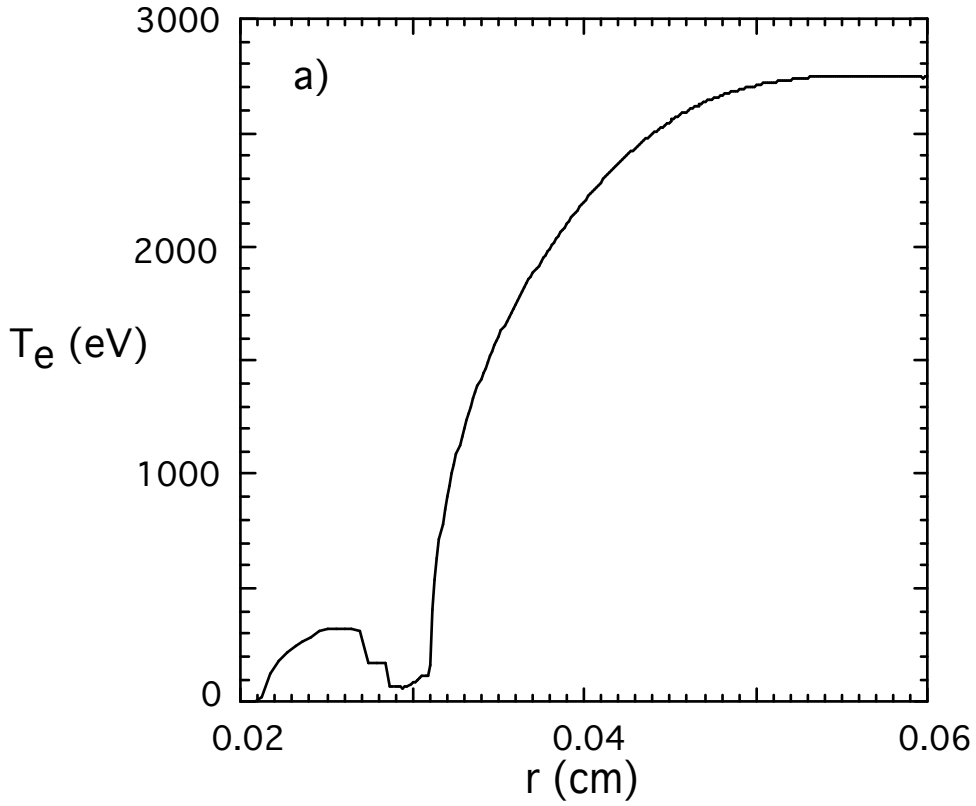

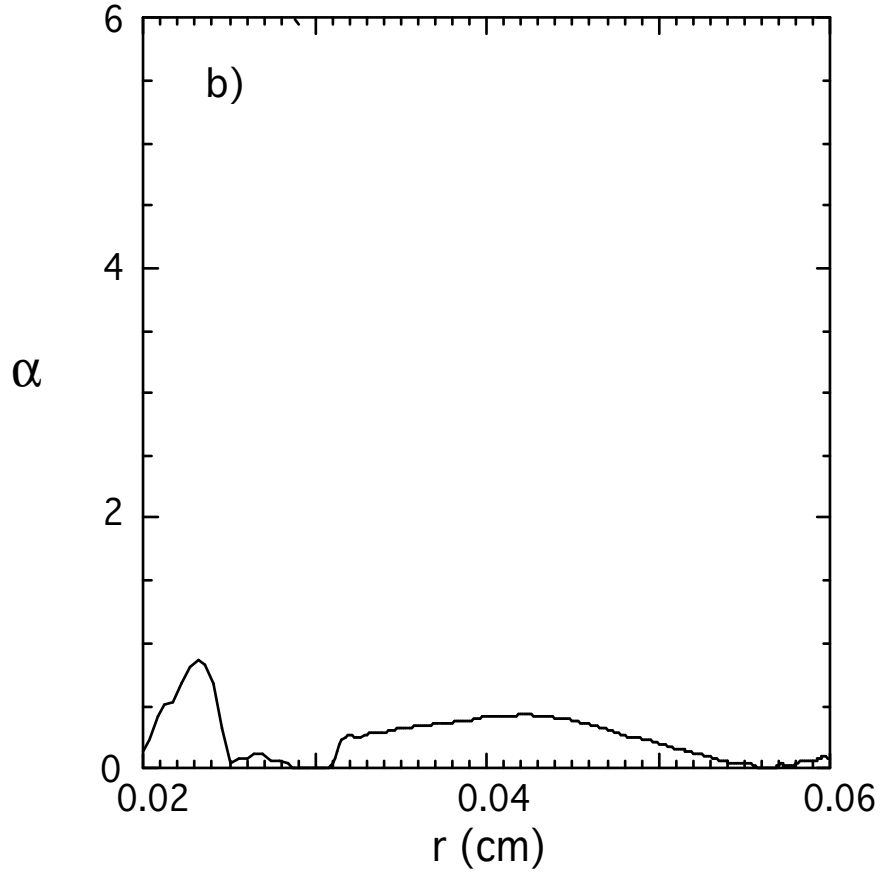

Fig. 5

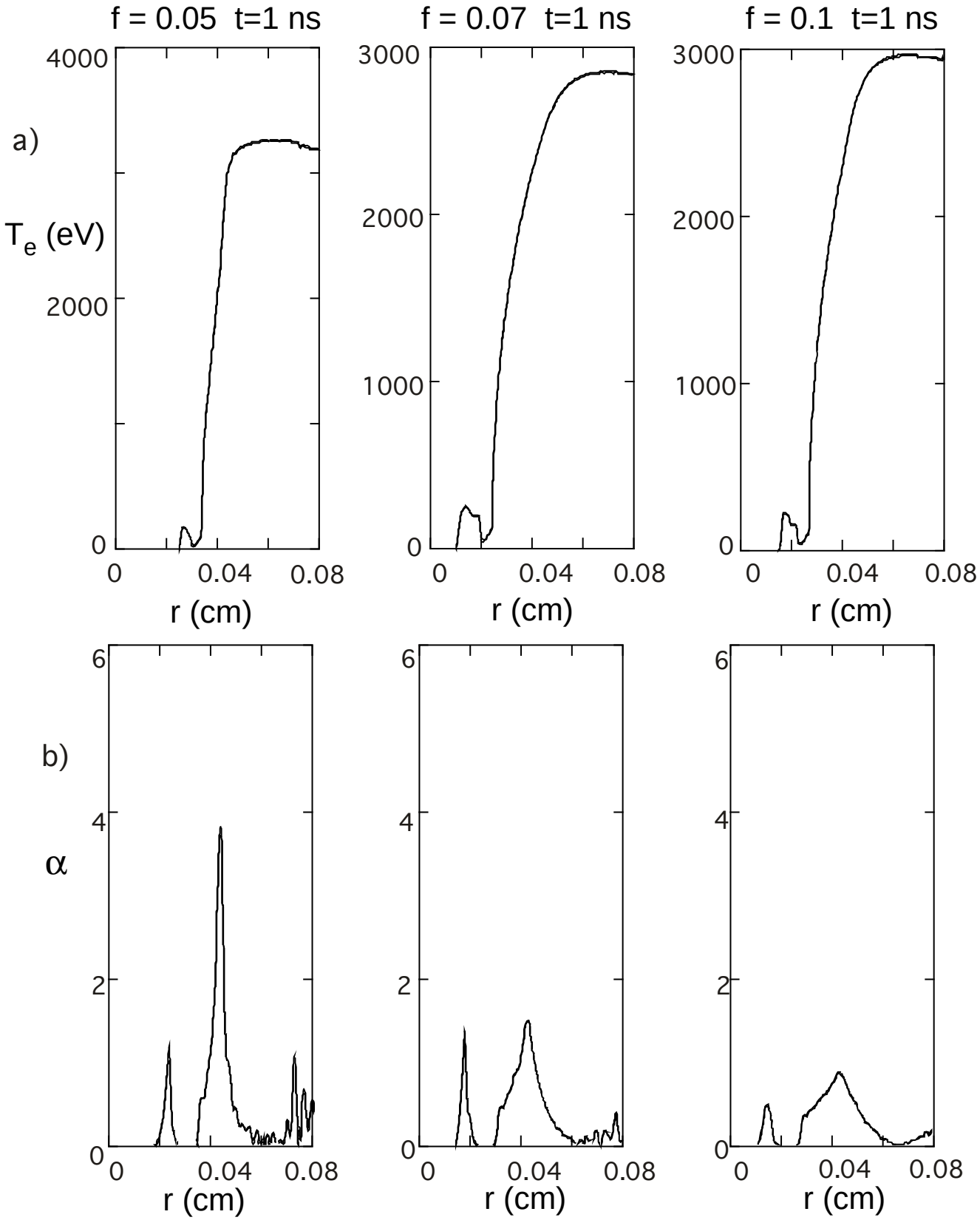
f = 0.05 t=1 ns
f = 0.07 t=1 ns
f = 0.1 t=1 ns
a)
T_e (eV)
4000
2000
0
3000
2000
1000
0
0
0.04
0.08
r (cm)
b)
α
6
4
2
0

Fig.6

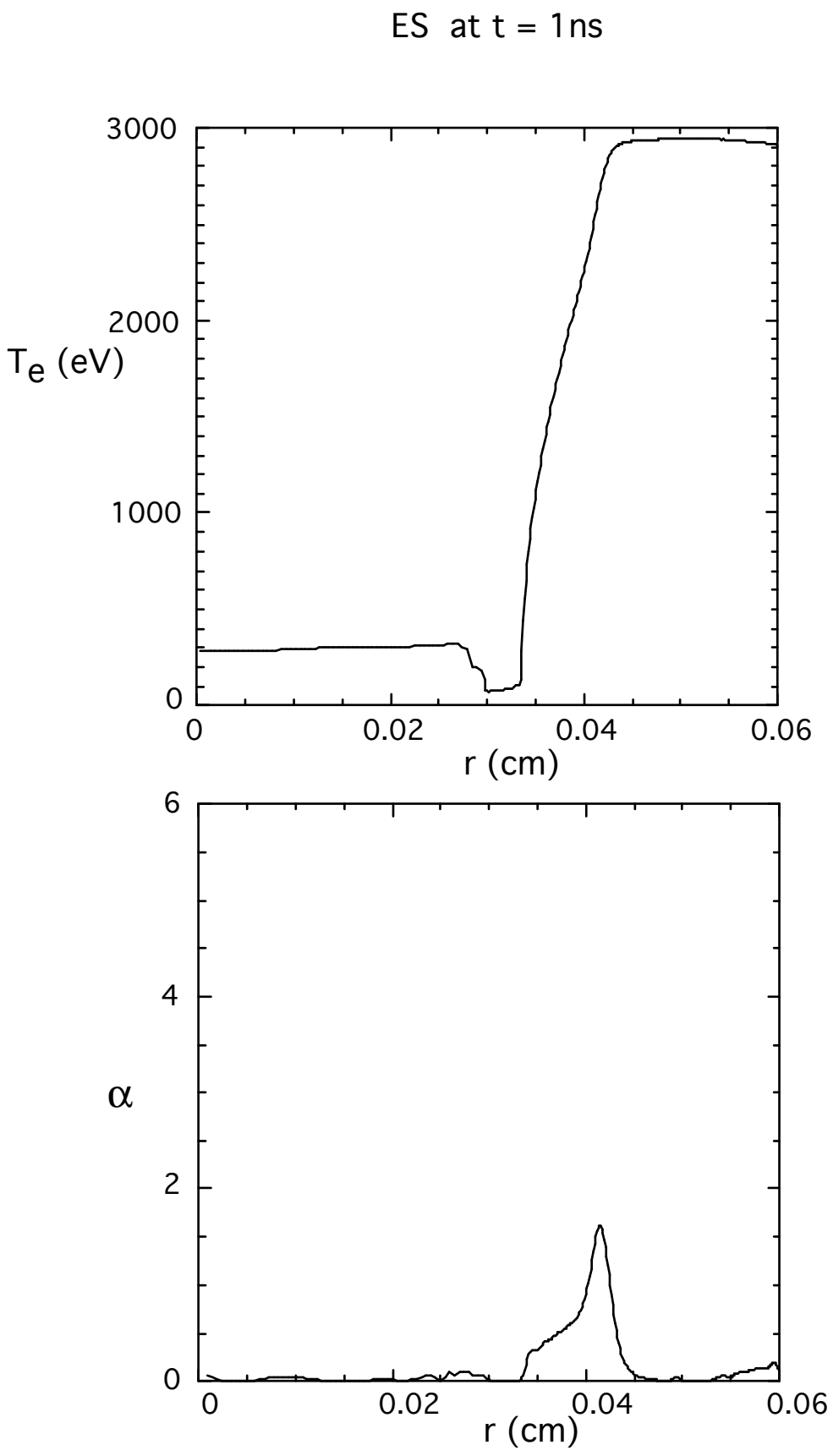
ES at t = 1ns
3000
2000
1000
0
T_e (eV)
0
0.02
0.04
0.06
r (cm)
6
4
2
0
α
0
0.02
0.04
0.06
r (cm)

Fig.7

Qsh vs. r for ES at t= 1ns

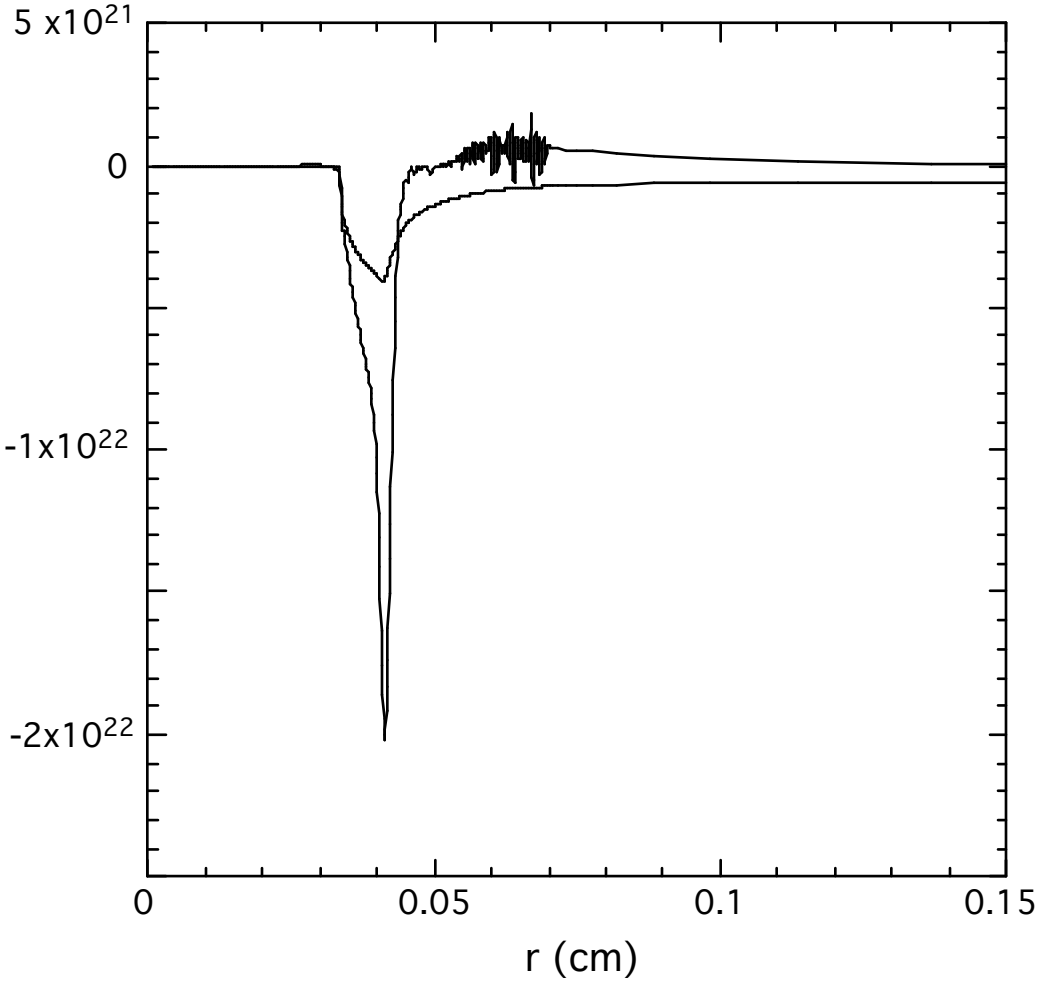

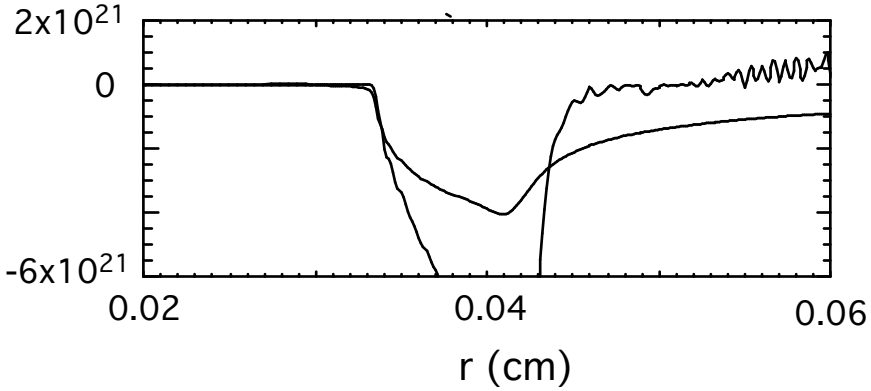

Fig.8

Beam deposition at t= 1ns

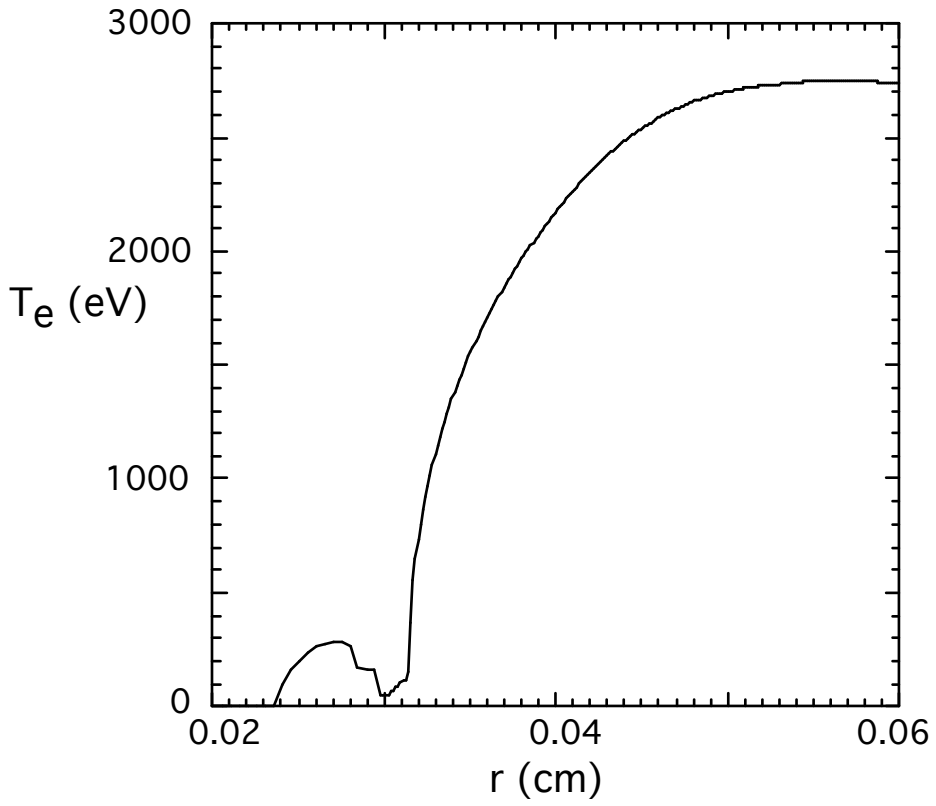

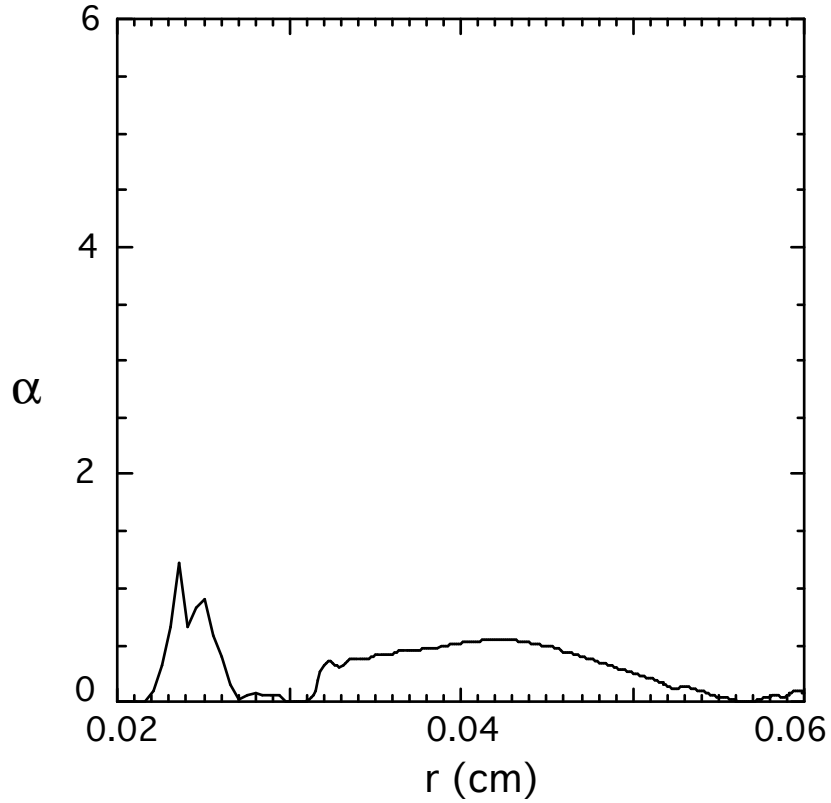

Fig.9

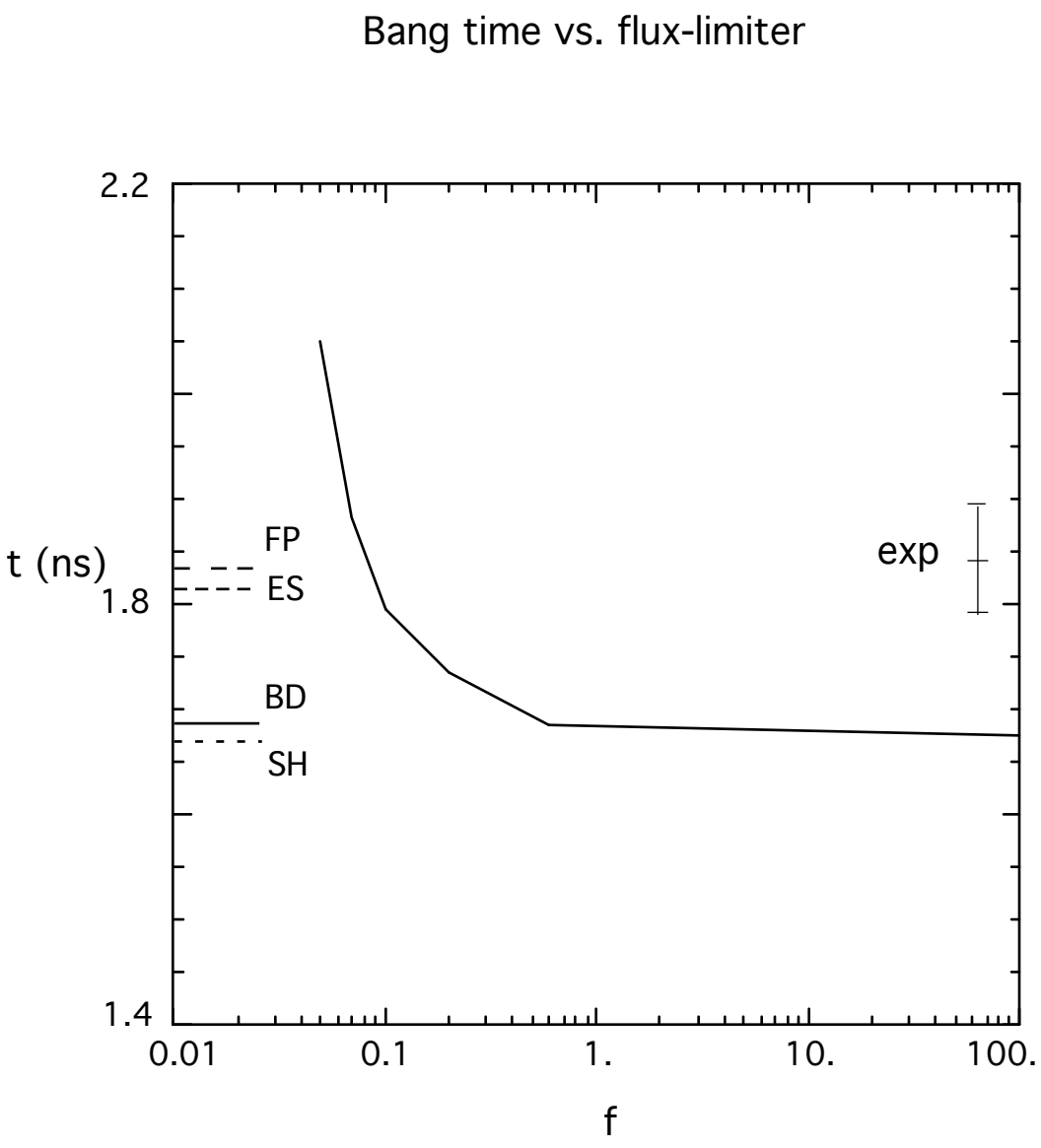
Bang time vs. flux-limiter
2.2
1.8
1.4
t (ns)
FP
ES
BD
SH
exp
0.01
0.1
1.
10.
100.
f

Fig.10

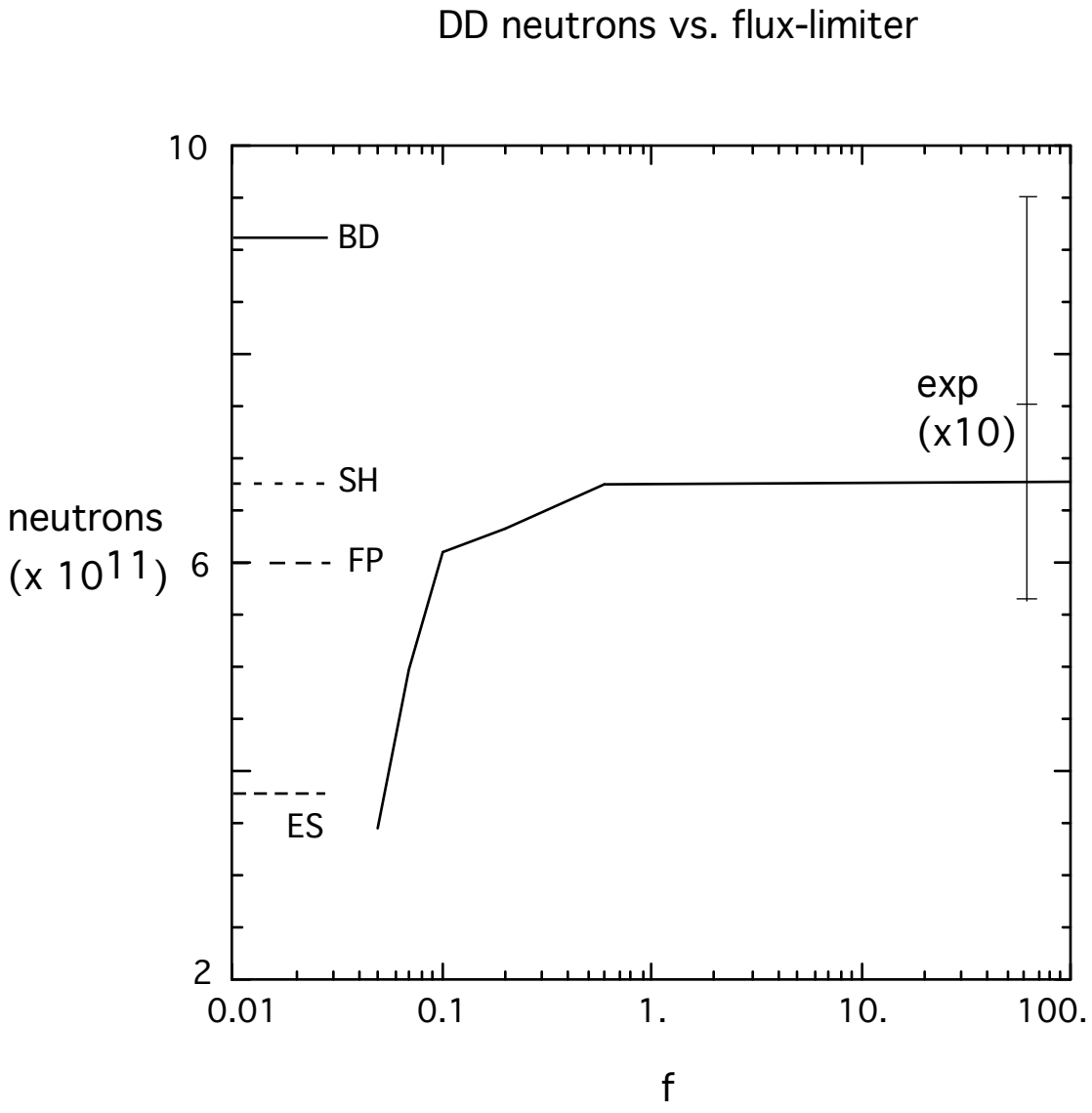
DD neutrons vs. flux-limiter
10
6
2
BD
SH
FP
ES
exp
(x10)
neutrons
(x 10^11)
0.01
0.1
1.
10.
100.
f

Fig.11

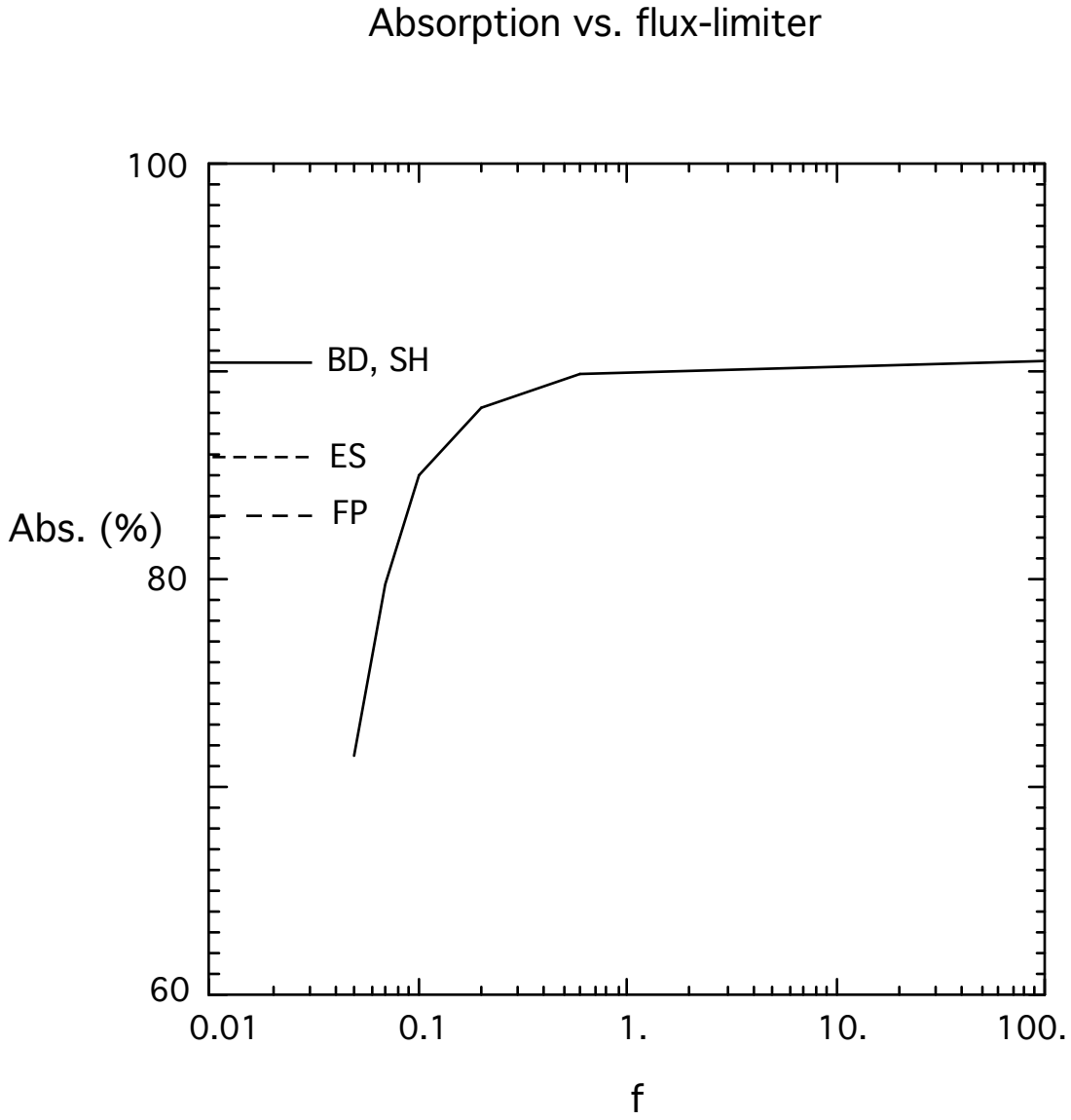
Absorption vs. flux-limiter
100
80
60
Abs. (%)
BD, SH
ES
FP
0.01
0.1
1.
10.
100.
f

Fig.12

Beam deposition

Profiles every 0.5 ns between 13 and 16 ns

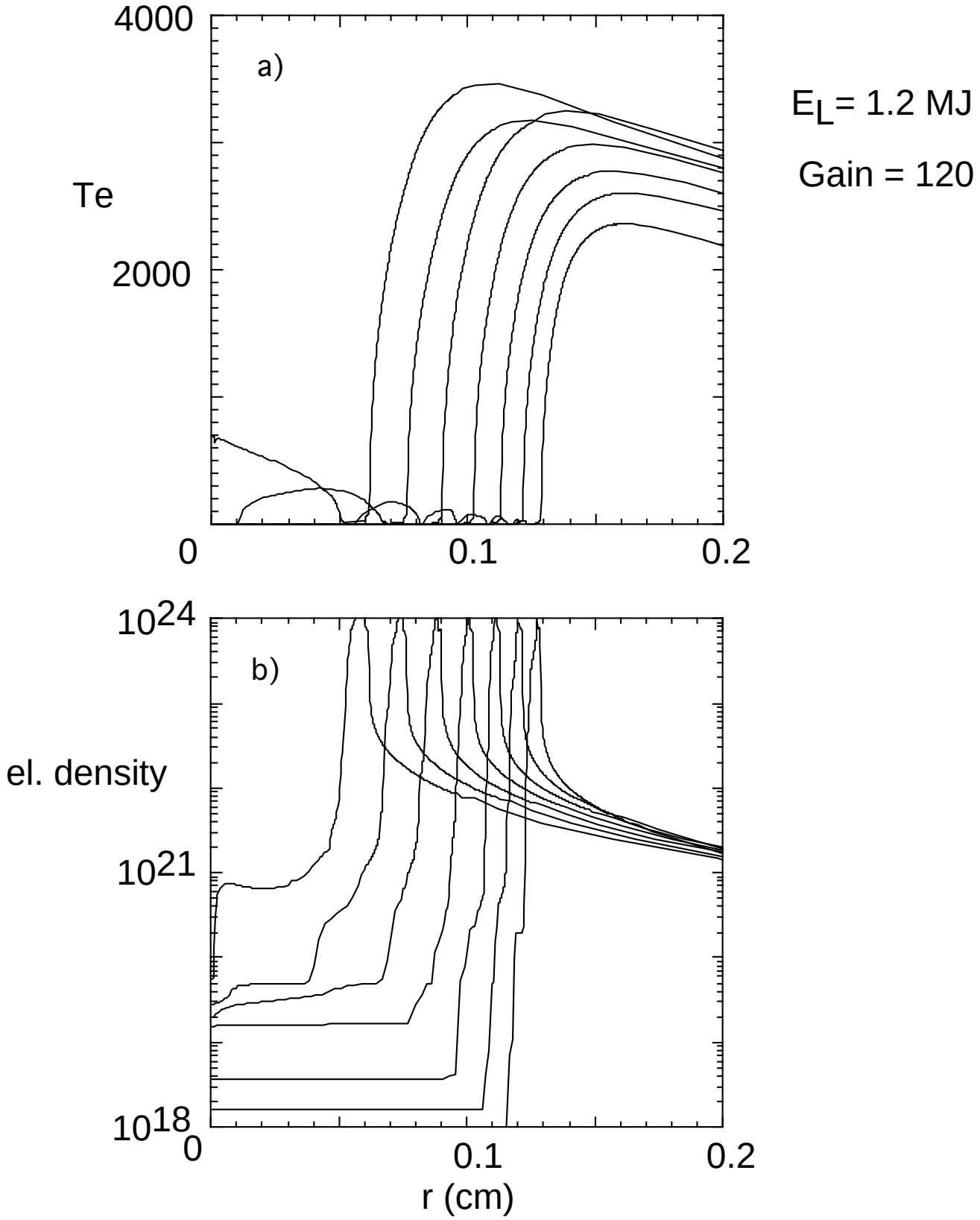

Fig.13

Delocalization model (ES)

Profiles every 0.5 ns between 13 and 16 ns

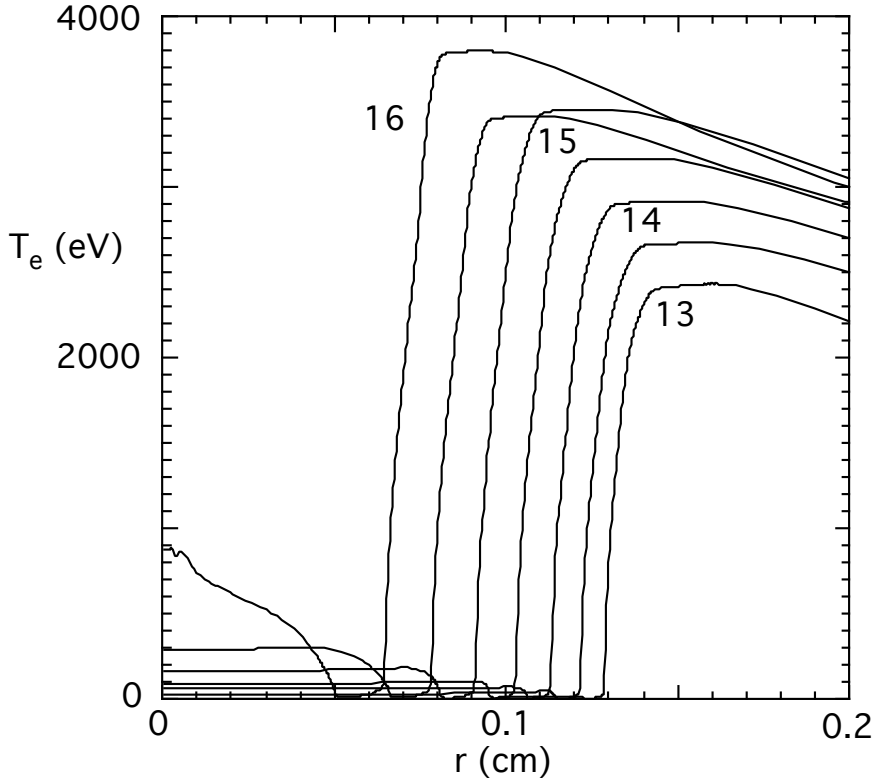

E_L=1.2 MJ

Gain=2.2

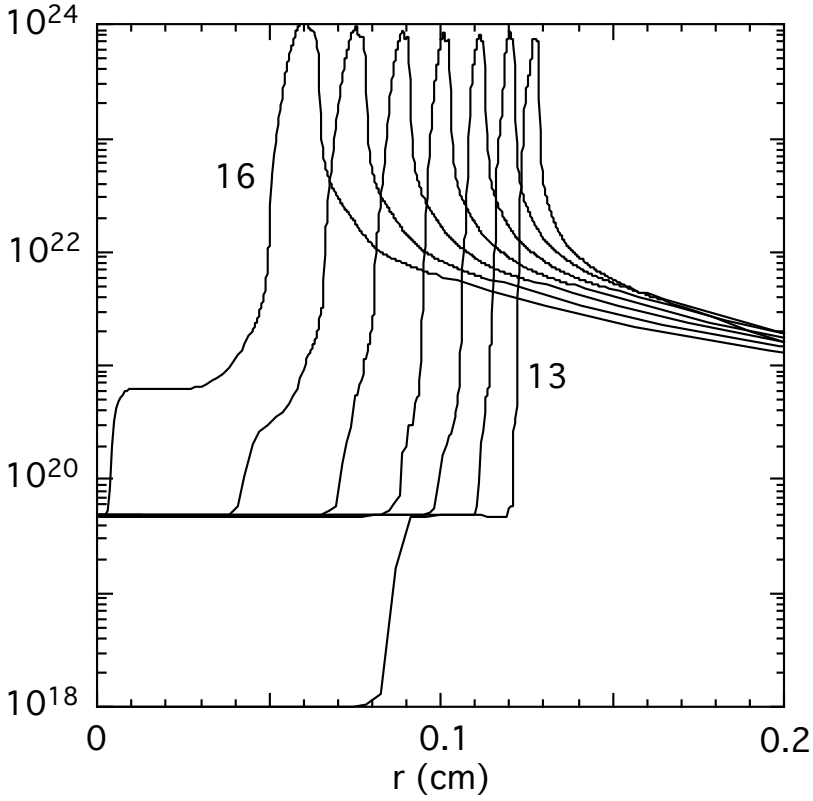

Fig.14

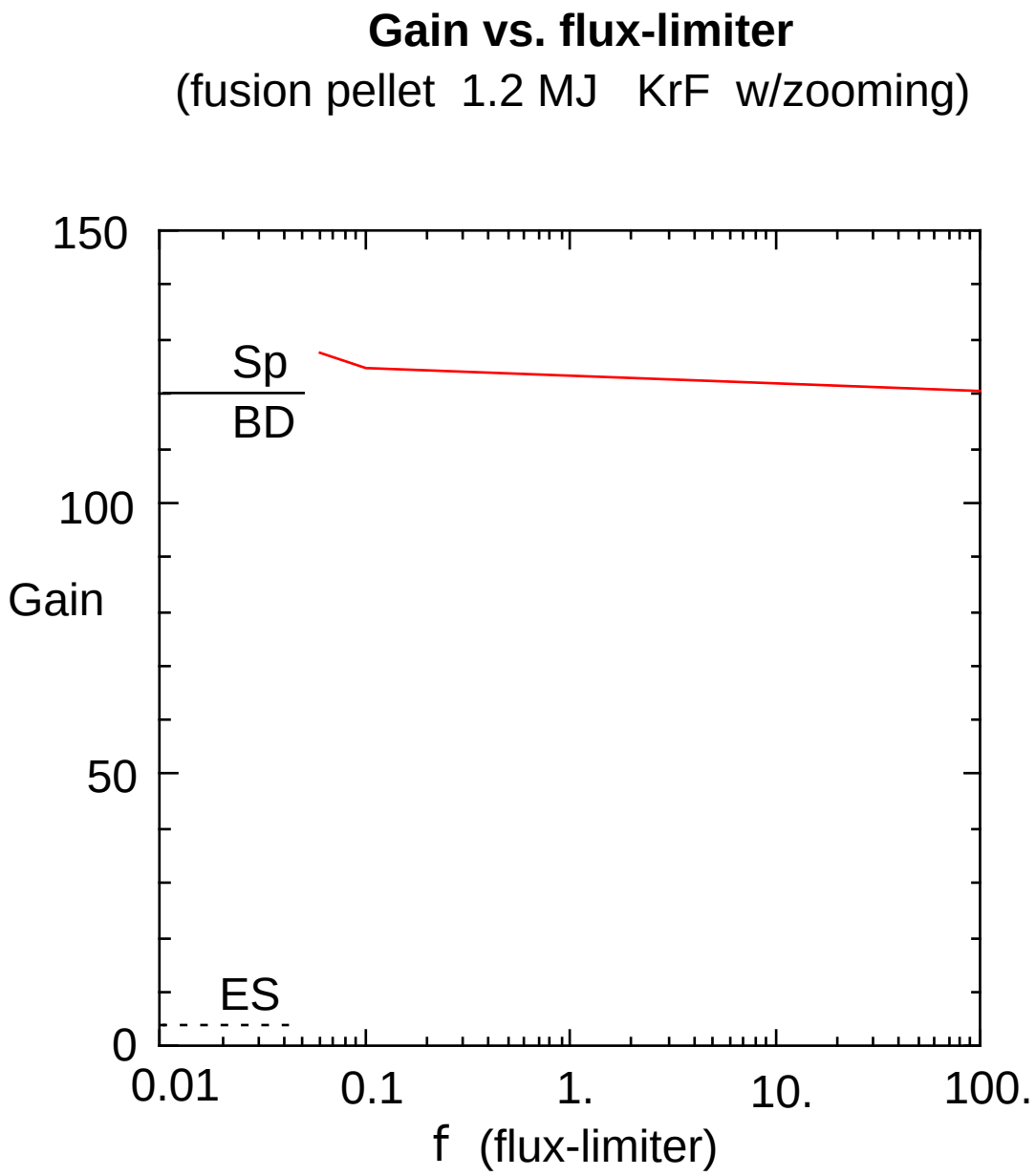
Gain vs. flux-limiter
(fusion pellet 1.2 MJ KrF w/zooming)
150
100
50
0
Gain
Sp
BD
ES
0.01
0.1
1.
10.
100.
f (flux-limiter)

Fig.15

Maximum α vs. flux-limiter value for fusion targets

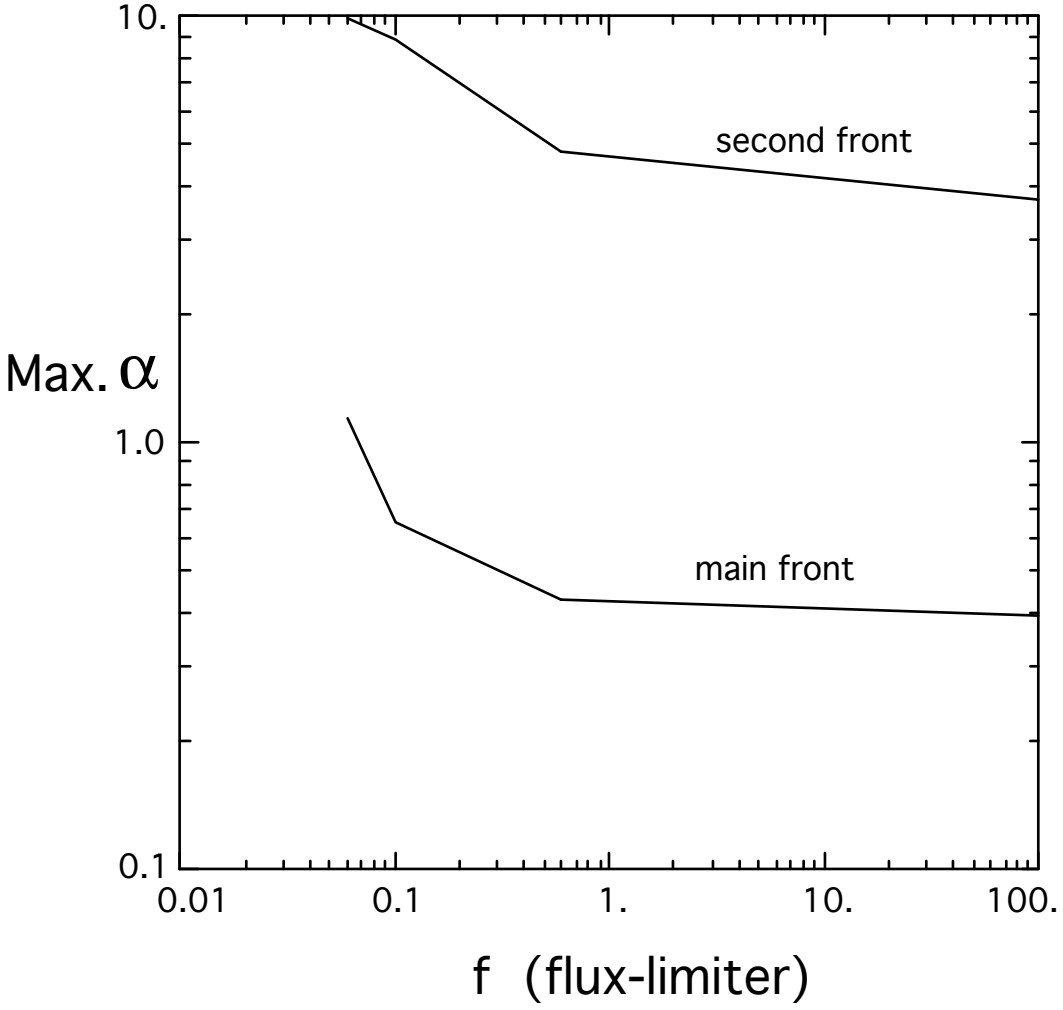

Fig.16

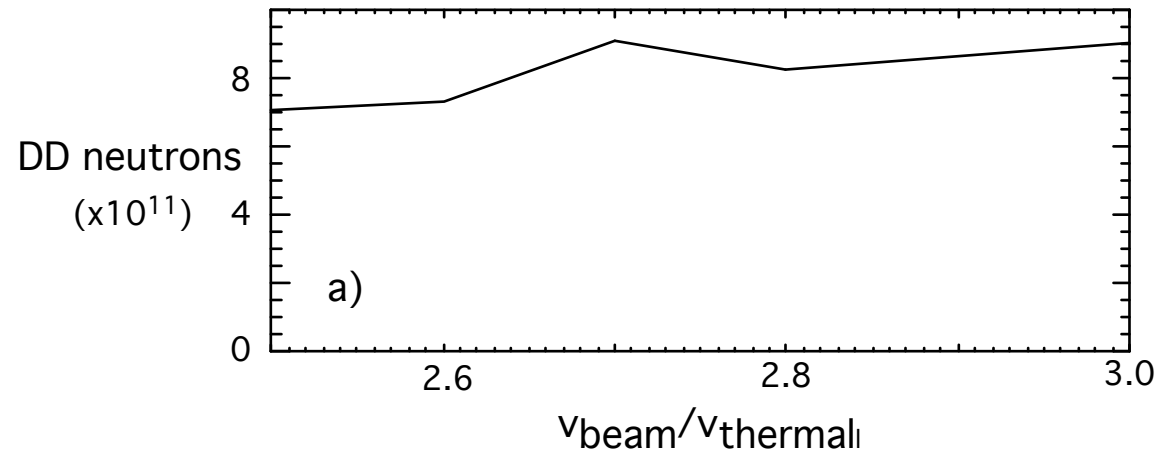
DD neutrons
(x10^11)
8
4
0
a)
2.6
2.8
3.0
v_beam/v_thermal

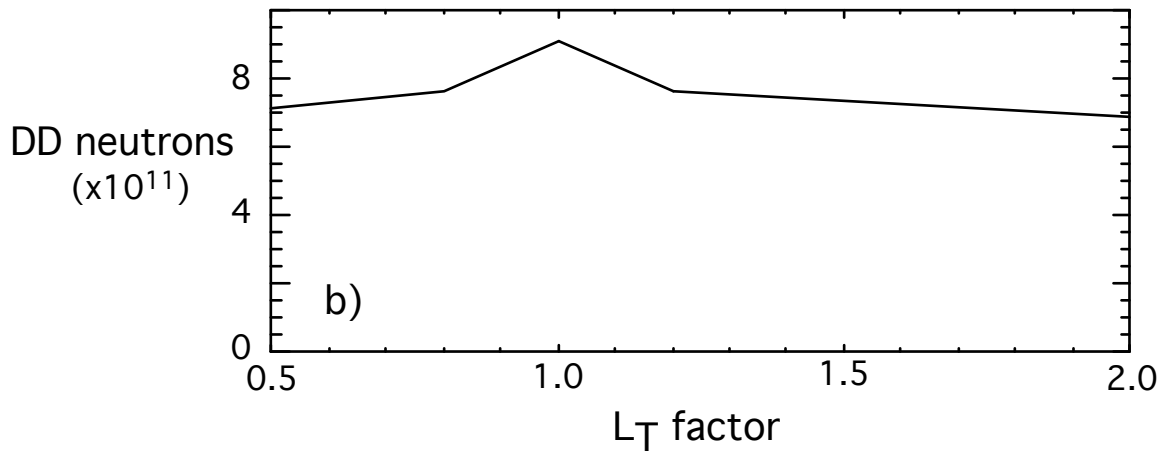
DD neutrons
(x10^11)
8
4
0
b)
0.5
1.0
1.5
2.0
L_T factor

1.0

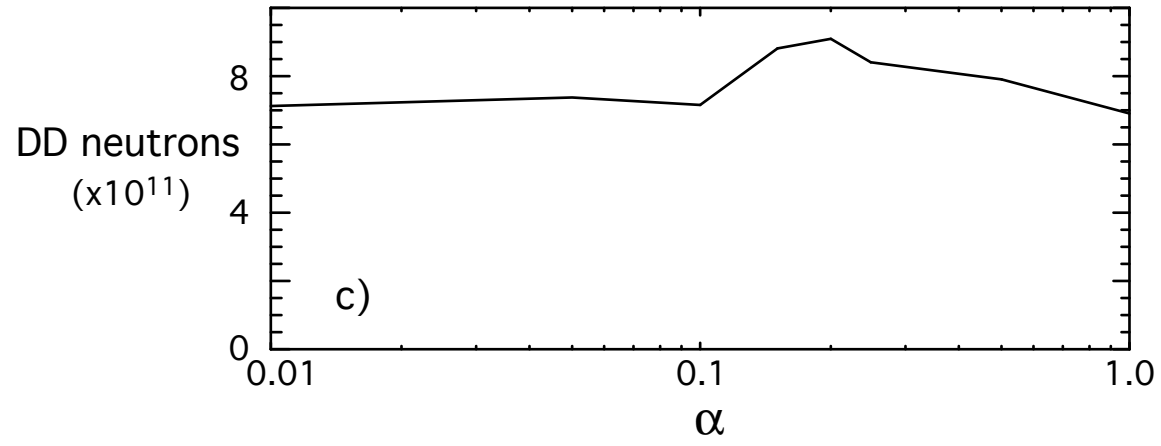
DD neutrons
(x10^11)
8
4
0
c)
0.01
0.1
1.0
α